北京航空航天大学四年级博士生和五年级直博生

学校奖学金申报表

（请按填表说明填写，本表填写的内容必须为非涉密可公开!）

<table>
<tr><td>姓　名</td><td>孙磊</td><td>学　号</td><td>BY1510109</td><td>指导教师</td><td colspan="2">牛旭锋</td></tr>
<tr><td>类　别</td><td colspan="3">√ 三年级博士生　□ 四年级直博生</td><td>学科/专业</td><td colspan="2">生物医学工程/生物材料</td></tr>
<tr><td rowspan="2">承担科研任务情况</td><td colspan="2">项目名称</td><td>课题来源</td><td>课题负责人</td><td colspan="2">本人承担的具体工作</td></tr>
<tr><td colspan="2">可降解生物材料不同特征化学官能团的体内外力化学降解机理研究</td><td>国家自然科学基金委</td><td>牛旭锋</td><td colspan="2">项目主研人员</td></tr>
<tr><td rowspan="11">已取得研究成果（论文、专利、获奖等）</td><td colspan="2">论文题目</td><td>本人排名</td><td>发表年月</td><td>期刊（会议）名称</td><td>被检索类型</td></tr>
<tr><td colspan="2">Development of Itraconazole Liquisolid Compact Effect of Polyvinylpyrrolidone on the Dissolution Properties.</td><td>2</td><td>2016 年 2 月</td><td>Current Drug Delivery</td><td>SCIE 源</td></tr>
<tr><td colspan="2">Immune response of bovine sourced cross-linked collagen sponge for hemostasis</td><td>3</td><td>2018 年 2 月</td><td>Journal of Biomaterials Applications</td><td>SCIE 源</td></tr>
<tr><td colspan="2">可吸收胶原膜的体内免疫反应评价</td><td>2</td><td>2018 年 4 月</td><td>北京航空航天大学学报</td><td>EI 源</td></tr>
<tr><td colspan="2">专利名称</td><td>本人排名</td><td>发布年月</td><td>专利号</td><td>专利类型</td></tr>
<tr><td colspan="2"></td><td></td><td></td><td></td><td></td></tr>
<tr><td colspan="2">获科技成果奖励名称</td><td>本人排名</td><td>获奖年月</td><td>证书编号</td><td>奖励级别</td></tr>
<tr><td colspan="2"></td><td></td><td></td><td></td><td></td></tr>
<tr><td>本人承诺</td><td colspan="6">本人所填写的以上内容均为真实情况。
本人签字：_____
年　月　日</td></tr>
<tr><td>导师意见</td><td colspan="6">同意 / 不同意 该同学申报学校奖学金。
导师签字：_____
年　月　日</td></tr>
<tr><td>学院学位评定分委员会意见</td><td colspan="6">同意 / 不同意 该同学获得学校奖学金。
签字：_____（学院代盖）
年　月　日</td></tr>
</table>

Current Drug Delivery, 2016, *13*, 452-461

Development of Itraconazole Liquisolid Compact: Effect of Polyvinylpyrrolidone on the Dissolution Properties

Wei Gong[1,#], Yuli Wang[1,#], Lei Sun[1,2,3], Jiahui Yang[1], Li Shan[1], Meiyan Yang[1,*] and Chunsheng Gao[1,*]

C. Gao

[1]State key Laboratory of Toxicology and Medical Countermeasures, Beijing Institute of Pharmacology and Toxicology, Beijing, China; [2]Key Laboratory for Biomechanics and Mechanobiology of Ministry of Education, School of Biological Science and Medical Engineering, Beihang University, Beijing, China and [3]Pharmaceutical College, Henan University, Kaifeng, China

M. Yang

Abstract: The aim of this work was to utilize the liquisolid technique to enhance dissolution of itraconazole (ITZ). Liquisolid tablets of ITZ were formulated by using N-methyl-2-pyrrolidone as liquid vehicle, polyvinylpyrrolidone (PVP) as a precipitation inhibitor and magnesium aluminometasilicate Neusilin® as a carrier and coating material. The effect of PVP level on stability of liquid medication, physicomechnanical properties and dissolution rate of liquisolid compacts was studied in detail. The crystallinity of formulated drug and the interaction between excipients were examined by differential scanning calorimetry (DSC) and X-ray powder diffraction (XRPD). All the liquisolid tablets showed higher drug dissolution rates than the conventional, directly compressed tablets. The flowability of liquisolid powders was slightly improved as the proportion of PVP in ITZ-NMP mixture increased. Moreover, the stability of liquid medication and wetting ability of liquisolid tablets were improved by PVP. The presence of low amount of PVP (≤ 1%) in liquisolid formulation could enhance dissolution of ITZ liquisolid tablets, whereas the percentage of PVP over 5% decreased the dissolution of ITZ from liquisolid tablets. Both DSC and XRPD suggested reduction or loss of ITZ crystallinity upon liquisolid formulations indicating that the drug was almost solubilized and molecularly dispersed with excipients within the liquisolid matrix. It could be shown that increased solubility, wetting properties and surface area available for dissolution contributed to the improvement of the dissolution of ITZ from liquisolid tablets.

Keywords: Dissolution, itraconazole, liquisolid compact, N-methyl-2-pyrrolidone, PVP.

Received: December 10, 2015 **Revised: January 01, 2016** **Accepted: February 02, 2016**

1. INTRODUCTION

Over 40% of active pharmaceutical ingredients (API) in development pipelines are poorly water-soluble drugs [1]. The great majority of these compounds can be classified according to the Biopharmaceutics Classification System (BCS) into BCS classes II, which are poorly soluble and highly permeable. Despite their high permeability, the low aqueous solubility of the drug in this class often leads to poor oral bioavailability because of their slow and limited release of drug in gastrointestinal fluid [2]. Therefore, one of the major challenges in drug development is to improve the solubility and/or dissolution of BCS class II drugs in order to enhance the bioavailability of these drugs. Various strategies to overcome the poor aqueous solubility of drug candidates have been investigated in drug research and development [3].

Itraconazole (ITZ) is a triazole antifungal agent against a broad spectrum of fungal species and effective for the treatment of both systemic fungal infections and superficial mycoses [4]. ITZ is classified as a BCS II drug due to its low aqueous solubility and high permeability. The aqueous solubility of ITZ is about 1 ng/ml at neutral pH and approximately 4 μg/ml in hydrochloric acid at pH 1 [5]. Its poor aqueous solubility makes the development of a sufficiently bioavailable ITZ formulation a challenge. Nowadays, only one intravenous formulation (Sporanox® injection) and two oral formulations (Sporanox® capsules and Sporanox® oral solution) are available. In order to improve the solubility and/or dissolution and ultimately the absorption, various drug delivery systems have been developed for oral, intravenous and topical administration, *e.g.*, solid dispersions [6], nano-amorphous powder [7], nanoparticles [8], nanosuspensions [9], nanospheres [10], transfersomes [11], liposomes [12], emulsions [13] and polymeric micelles [14].

For oral delivery of poorly soluble drugs, in addition to solid dispersions, a new technique of "liquisolid compacts" is one of the most promising techniques [15-17]. Liquisolid systems refer to formulations formed by conversion of liquid drugs, drug suspensions or drug solution in non-volatile solvents into dry, nonadherent, free-flowing and compressible and compactible powder mixtures by blending the suspen-

*Address correspondence to these authors at Beijing Institute of Pharmacology and Toxicology, Beijing 100850, China; Tel: +86-10-66931638; E-mail: ymyzi@163.com; and Tel: +86-10-66931638;
E-mail: gaocs@bmi.ac.cn

[#] These authors contributed equally to this work.

1875-5704/16 $58.00+.00

sion or solution with selected carriers and coating materials [18]. The poorly soluble drugs in liquisolid systems might be in a solubilized, almost molecularly dispersed state [16]. Therefore, the enhanced drug release properties, and consequently, improved bioavailability by liquisolid systems could be attributed to increased surface area of the drug, increased aqueous solubility, and improved wettability of drug particles [19, 20]. Liquisolid technique was successfully applied for many water-insoluble drugs.

However, formulation liquisolid tablet of high dose lipophilic drugs is one of the limitations of this technique. Liquisolid system of ITZ has not been reported so far. In order to achieve acceptable flowability and compactibility for liquisolid formulation, high levels of carrier material and coating materials should be added. This will increase the weight of tablets to above one gram which makes them difficult to swallow [21]. A potential approach to minimize tablet weight is to choose suitable non-volatile solvents possessing high solution capacity to minimize the required amount of liquid vehicle. Meanwhile, the liquid adsorption capacity can be enhanced by using carrier and coating materials with a high specific surface area (SSA). The higher the SSA of an excipient, the higher the liquid load factor [22]. Moreover, some polymer excipients, such as hydroxypropylmethylcellulose (HPMC) and polyvinyl pyrrolidone (PVP), were found to be useful in generating a supersaturated state with a number of poorly soluble drugs [23, 24], and consequently reducing amount of liquid vehicle and increasing stability of supersaturated solution.

The aim of this work was to utilize the liquisolid technique to enhance dissolution of ITZ. N-methyl-2-pyrrolidone (a very strong solubilizing agent) and Neusilin® (porous granules with extremely high SSA and good flowability and tabletability) were used as liquid vehicle and carrier/coating material respectively for ITZ liquisolid system. Furthermore, PVP was added to liquid medication as a precipitation inhibitor. The effect of PVP concentration on stability of liquid medication, physicomechnanical properties and dissolution rate of liquisolid compacts were investigated in detail.

2. MATERIALS AND METHODS

2.1. Materials

Itraconazole was obtained from SMS Pharmaceuticals Ltd (India). Polyvinylpyrrolidone (PVP, Kollidon 30) and Cremophor® RH40 were obtained from BASF (Berlin, Germany). N-methyl-2-pyrrolidone (NMP) was purchased from Ashland Inc (KY, USA). Labrasol®, Plurol® Oleique CC 497 and Transcutol® HP were supplied by Gattefossé Corp., Saint-Priest, France. Croscarmellose sodium Vivasol® was obtained from JRS Pharma GmbH (Rosenberg, Germany). Neusilin® US2 (magnesium aluminometasilicate) was purchased from Fuji Chemical Industries Co., Ltd (Japan). Polyethylene glycol 400 (PEG 400) was purchased from Sasol Germany (Hamburg, Germany). Polysorbate 80 was obtained from Croda International Plc (East Yorkshire, UK). Propylene glycol was supplied by XiLong Chemical Co., Ltd (Shantou, China). Span 80 was obtained from Sinopharm Chemical Reagent Co., Ltd (Shanghai, China). The other excipients were of standard pharmaceutical grade and all chemical reagents used were of analytical or high-performance liquid chromatography (HPLC) grade.

2.2. Solubility Measurement

The solubility studies of ITZ in non-volatile solvents were performed in polyethylene glycol 400 (PEG 400), propylene glycol, span 80, Polysorbate 80, Labrasol®, N-methyl-2-pyrrolidone, Cremophor® RH40, Plurol® Oleique CC 497 and Transcutol® HP. Saturated solutions of ITZ were prepared by adding excess drug in a small flask containing above mentioned solvents. After 2 h ultrasound treatment, the flasks were rotated at 37°C for 72 h. The supernatants were filtered using 0.45 μm filter and further diluted with methanol. The drug concentration was determined by HPLC analysis with an Agilent HPLC system (Pump G1312B, UV detector G1316B, Autosampler 1367C, Degasser G1379B, Agilent Technologies, USA). The HPLC analysis conditions were as follows: reversed phase C_{18} analytical column (Diamonsil, 4.6 × 200 mm, 5 μm, Dikma Technologies Inc., Beijing, China); mobile phase, methanol-water (90:10, v/v); wavelength, 261nm; column temperature, 25 °C; flow rate, 1.0 mL/min.

2.3. Calculation of the Flowable Liquid-retention Potential (*Φ*-value) for Neusilin® US2 and the Loading Factor (L_f)

Powder excipient Neusilin® US2 was used as carrier material and coating material. The optimal flowable liquid-retention potential of Neusilin® US2 in NMP was calculated based on the angle of slide measurement. Powder admixtures containing 10 g Neusilin® US2 with increasing quantity of NMP were prepared and placed on one end of a polished metal plate, which was tilted gradually until the liquid/powder admixture started to slide. The angle formed between the plate and the horizontal surface was defined as the angle of slide (θ). The flowable liquid retention potential was calculated using the following equation. The *Φ-value* which corresponded to an angle of slide of 33° was reported to represent the flowable liquid retention potential of powder admixture [25].

$$\phi - \text{value} = \frac{\text{weight of NMP}}{\text{weight of Neusilin}} \quad \text{Eq. (1)}$$

The value of loading factor (L_f) was calculated as follows:

$$L_f = \phi_{ca} + \phi_{co} \times \frac{1}{R} \quad \text{Eq. (2)}$$

Where Φ_{ca} *and* Φ_{co} were carrier *Φ-value* and coating *Φ-value*, respectively. *R* was carrier/coating ratio.

2.4. Preparation of Liquisolid Compacts and Conventional Tablets

ITZ liquisolid formulations were prepared using NMP as liquid vehicles. All liquisolid formulations contained Neusilin® US2 as the carrier powder and coating material. The carrier/coating ratio (R) was chosen to be 20 for all liquisolid formulations. The amount of liquid medication (*W*) required for each formulation was determined according to the drug concentration in the liquid vehicle. The amount of

carrier (Q) and coating material (q) was calculated using equation (3) and (4). The formulation characteristics for each liquisolid system were summarized in Table **1**.

$$L_f = \frac{W}{Q} \quad \text{Eq. (3)}$$

$$R = \frac{Q}{q} \quad \text{Eq. (4)}$$

The desired quantity of the previously weighed ITZ and NMP were mixed with constant stirring in 90 °C water bath. Then various amount of PVP was added to drug mixture. The appropriate amount of drug-vehicle suspension was incorporated into the calculated quantities of the blend of carrier and coating material using a standard mixing process as described by Spireas *et al.* [26]. Finally, a 6% (w/w) of Vivasol® as a disintegrant was added into the mixture and mixed. The final mixture was compressed into tablet in ZP-5 rotary tablet press (Shanghai Tianhe Pharmaceutical Device Co., Ltd., China) using an 11 mm diameter punch to achieve tablet hardness of 56-70 N.

For comparison, conventional ITZ tablets (DCT-PM, 50 mg/tablet) were prepared by mixing the drug with Neusilin® US2 for a period of10 min. Granules were formulated by the same procedure of liquisolid formulation (Table **1**).

2.5. Stability Evaluation of Drug-vehicle Mixture

The stability of drug-vehicle mixture containing various amount of PVP was evaluated by a turbidity scanner (Turbiscan Lab® Expert, Formulaction, France). Turbiscan Lab® is an optical analyzer which is able to predict the potential destabilization of colloidal systems using the multiple light scattering analysis. 15 mL solution was filled into cylindrical glass cell and then analyzed. The detection head scanned the entire height of the sample, acquiring transmittance (T) and backscattering (BS) data over 24 h at 30 °C. The variation of the delta backscattering (ΔBS) was calculated as the difference between BS intensity at 0 h and at a given time. The raw data of T and BS were further processed using Turbiscan Lab® workstation and reported as turbiscan stability index (TSI) versus time.

2.6. Characterization of Liquisolid Powder

2.6.1. Flowability Measurement

The flowability of all liquisolid powders and physical mixtures were assessed based on Carr's compressibility index (CI), which depends upon tapped densities (P_t) and poured bulk densities (P_b) of the admixture. The prepared liquisolid powders or physical mixtures were weighed and poured into a cylinder on a tap volumeter. The poured bulk volume (V_b) and the tapped volume (V_t) after sufficient taps were recorded to calculate P_b and P_t. The *CI %* was calculated according to the following equation [27].

$$CI\,\% = \frac{P_t - P_b}{P_t} \times 100 \quad \text{Eq. (5)}$$

2.6.2. Differential Scanning Calorimetry (DSC)

DSC was performed in order to assess the thermotropic properties and the thermal behaviors by using differential scanning calorimeter (Q-2000, TA, New Castle, DE, USA). ITZ, PVP, Neusilin® US2, physical mixtures and liquisolid powders were weighed in a standard open aluminum pan with an identical empty pan used as a reference. The heating program was set to run from 40 °C to 260 °C at 10 °C/min for each sample, while using nitrogen as a purge gas. The temperature and heat flow calibrations were performed with indium.

2.6.3. X-ray Powder Diffraction (XRPD)

The X-ray powder diffraction (XRPD) patterns were determined for ITZ, PVP, Neusilin® US2, physical mixtures and liquisolid powders with a diffractometer (D8 Advance, Brucker, Karlsruhe, Germany) using Cu-Kα radiation at 40 kV and 40 mA. The samples were scanned in increments of 0.015° from 6° to 55° (diffraction angle 2θ) at 0.4 s per step while using a zero background sample holder.

2.7. Evaluation of ITZ Liquisolid Formulations

2.7.1. Measurement of Contact Angle

The contact angle measurements were performed on a goniometer (OCA20, Dataphysics Instruments GmbH,

Table 1. Formulation characteristics of liquisolid systems and conventional formulation.

Formula	Total drug content in liquid portion (%, w/w)	Amount of PVP in liquid portion (%, w/w)	Amount of carrier and coating blend (mg)	Disintegrant (mg)	Unit dose (mg)
LS-LC	7.1	0	234.5	26.2	495.4
LS-PVP-0%	22.8	0	291.9	32.6	543.5
LS-PVP-0.5%	22.8	0.5	293.3	32.7	546.2
LS-PVP-1%	22.8	1	294.9	32.9	549.0
LS-PVP-5%	22.8	5	307.3	34.3	572.1
LS-PVP-10%	22.8	10	324.3	36.2	603.9
LS-PVP-20%	22.8	20	364.9	40.7	679.4
DCT-PM	-	-	291.9	21.8	363.7

Filderstadt, Germany) using sessile drop technique. A droplet of 0.1 M hydrochloric acid solution was placed onto the surface of the tablet and observed immediately through a lowpowder microscope until the drop reached a quasi equilibrium shape. The contact angle was determined by measuring the tangent of the droplet on the tablet.

2.7.2. Dissolution Studies

In vitro release test was performed according to USP paddle method using a USP dissolution apparatus (SR8PLUS dissolution tester, Hanson Research Corporation, Chatsworth, CA). The dissolution medium used was 1000 mL of 0.1 M hydrochloric acid, maintained at 37 °C, and the paddle speed was 75 rpm. Samples of 8 ml taken at predetermined time intervals were filtered through a 0.45 μm filter. The drug content in sample was determined using UV/Vis spectrophotometer (Model UV-1750, Shimadzu Corporation, Kyoto, Japan) at 262 nm.

2.8. Statistical Analysis

Levene's test was applied to test the homogeneity of variances. One-way ANOVA and independent-samples T-test were applied if the variances in the groups are equal. If the variances are significantly different, Mann–Whitney test was applied. Results are quoted as statistically significant when $P < 0.05$.

3. RESULTS AND DISCUSSION

3.1. Solubility Measurement

The solubility of ITZ in various non-volatile solvents was determined and presented in Table **2**. The solubility results showed that ITZ was poorly soluble in several commonly used non-volatile solvents. ITZ had significantly higher solubility in NMP (92.95 ± 1.35 mg/ml) compared to other solvents. NMP is one of the main pharmaceutical solubilizing agents used in parenteral and oral medications. It is proposed that NMP enhances drug solubility by simultaneously acting as a cosolvent, complexing agent and surfactant [28, 29].

Drug solubility in a non-volatile vehicle is the most important aspect in liquisolid systems. The solubility of the drug contributed to molecular dispersion in non-volatile solvent which will improve the dissolution rate [30]. Therefore, the liquid vehicle in which the drug has the highest solubility is supposed to enhance rate of drug dissolution the most [31]. Furthermore, suitable non-volatile solvents possessing high solution capacity may reduce the required amount of carrier and coating materials. Therefore, NMP was chosen as liquid vehicle for preparation of ITZ liquisolid compacts based on the solubility data.

Table 2. Solubility of itraconazole in various non-volatile solvents.

Solvent	Solubility (mg/ml)
PEG 400	3.11 ± 0.12
Propylene glycol	0.24 ± 0.02
Span 80	13.41 ± 0.31
Polysorbate 80	2.89 ± 0.09
N-methyl-2-pyrrolidone	92.95 ± 1.35
Cremophor® RH40	3.18 ± 0.09
Labrasol®	2.73 ± 0.10
Plurol® Oleique CC 497	7.52 ± 0.15
Transcutol® HP	5.06 ± 0.13

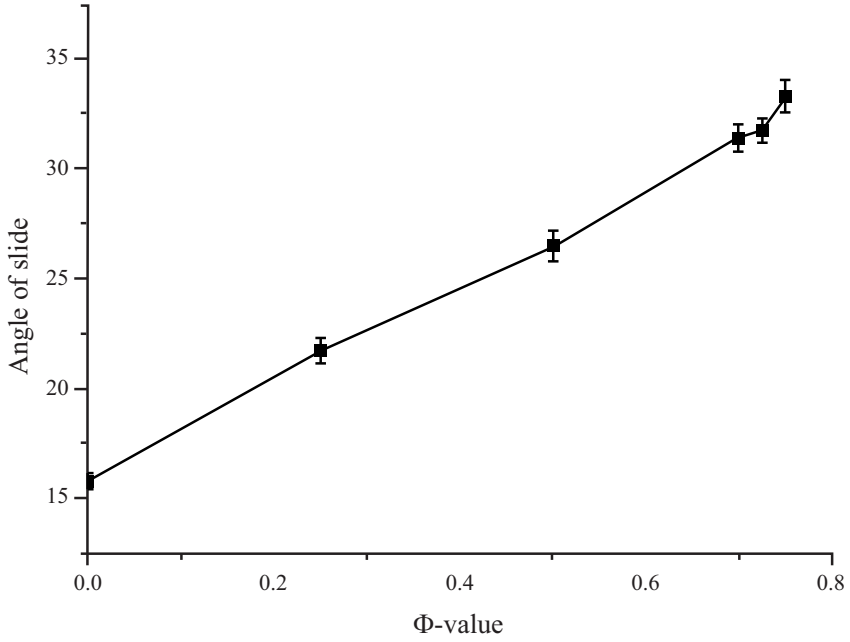

Fig. (1). The angle of slide of mixtures of Neusilin® US2 with N-methyl-2-pyrrolidone. The intersection of each curve with horizontal dashed line at 33° represents the *Φ*-value.

3.2. Flowable Liquid-retention Potential (*Φ*-value) and Loading Factor (L_f)

Carrier and coating materials strongly affect the liquid adsorption capacity of liquisolid formulations. Neusilin® US2, a synthetic amorphous form of magnesium aluminometasilicate, was selected as carrier and coating materials for preparation of ITZ liquisolid compacts due to its extremely high SSA and good flowability and tabletability [22]. In order to calculate the loading factor, the flowable liquid-retention potential of Neusilin® US2 in NMP was determined by angle of slide determination. The relationship between the angle of slide and corresponding *Φ*-value for Neusilin® US2 in NMP was illustrated in Fig. (**1**). The *Φ*-value of Neusilin® US2 in NMP was 0.75. Then the L_f was calculated and used to decide the optimum amount of carrier and coating materials required to produce liquisolid formulations (Table **1**).

3.3. Stability Evalutions of Drug-vehicle Mixture

The influences of PVP on the stability of ITZ-NMP liquid medication was studied using Turbiscan Lab®. A typical example of the backscattering as a function of time and sample height was shown in Fig. (**2a**) and Fig. (**2b**) for the drug-vehicle mixture containing 0% and 20% PVP, respectively. It was noticed that the variation of *ΔBS* of the ITZ-NMP mixture containing 20% PVP was evidently smaller than that of the ITZ-NMP mixture without PVP. The stability kinetics calculated from the transmission and backscattering differential profiles was given in Fig. (**2c**). The value of turbiscan stability index (TSI) reflected the destabilization of a given sample. The higher the TSI, the stronger the destabilization in the sample. The TSI increased with the decrease of the proportion of PVP in ITZ-NMP mixture. The ITZ-NMP mixture containing 20% PVP was the most stable whereas the ITZ-NMP mixture containing 0% PVP was the most unstable.

In principle, high drug concentrations obtained by solubilization or supersaturable formulations lead to an increase in oral absorption. However, since drugs are thermodynamically unstable at high concentrations, they have a tendency to precipitate rapidly *in vivo* before being absorbed, resulting in compromised bioavailability [32]. ITZ molecules in highly concentrated solution without PVP had the tendency to precipitate [33]. The crystallization and precipitation of ITZ may be the primary influencing factor of stability of ITZ-NMP mixture. In order to maintain drug at a high concentration for an extended period of time, precipitation inhibitors have been widely explored for temporary inhibition of drug precipitation [34]. PVP was a frequently used polymer precipitation inhibitor in supersaturating drug delivery systems [35-37]. According to the stability results, the presence of PVP in liquid medication may stabilize ITZ supersaturation by suppressing the drug nucleation process [24, 38].

3.4. Characterization of Liquisolid Powder

3.4.1. Flowability Measurement

Powder flowability is crucial in the industrial production of tablet dosage forms to ensure that the flow of the powder from hopper to die cavity is uniform and reproducible in order to obtain uniform tablet weight and drug content. Carr's index

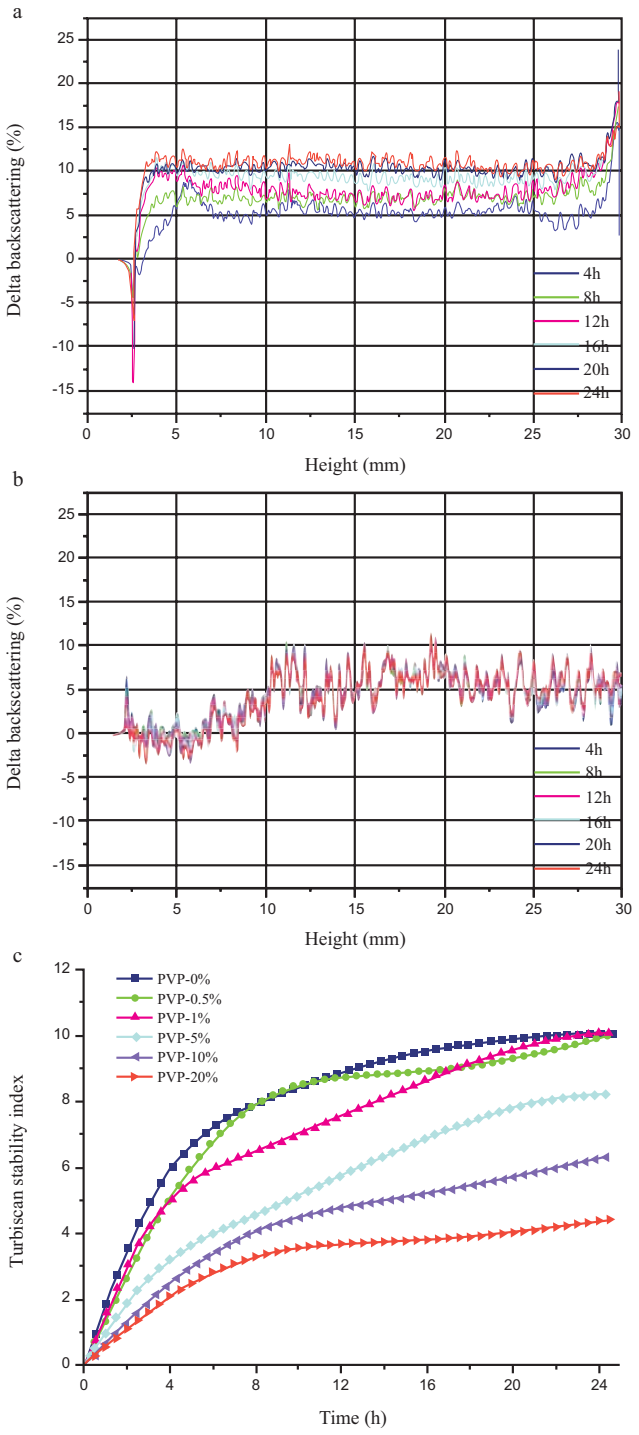

Fig. (2). Delta backscattering *ΔBS* evolution as a function of time and sample height for ITZ-NMP mixture containing 0% (**a**) and 20% (**b**) PVP, and the stability kinetics profiles (turbiscan stability index, TSI) of ITZ-NMP mixture containing various amount of PVP (**c**) using Turbiscan Lab®.

(*CI %*) is commonly used for evaluation of powder flow properties. The powder flowability of all liquisolid formulations and physical mixtures was determined using Carr's index as shown in Table **3**. All liquisolid powder except LS-PVP-20% had *CI %* below 25%, which indicated adequate flow properties. Moreover, the flowability of powders was

slightly improved as the amount of PVP in ITZ-NMP mixture increased. Because in all liquisolid formulation the *Lf* was the same, increase of PVP proportion in drug-vehicle mixture resulted in the increase of the amount of the carrier and coating materials. Moreover, the increased viscosity of the drug-vehicle mixture with the increase of PVP level (data not shown) made less carrier and coating materials needed to completely adsorb liquid [17]. Therefore, powder flowability was improved due to relatively large proportion of carrier and coating materials used. However, formulation LS-PVP-20% containing 20% PVP in drug-vehicle mixture showed poor flow properties compared to the other liquisolid formulations. This could be ascribed to the high viscosity of drug-vehicle mixture containing 20% PVP (about 6 times of that of mixture containing 10% PVP, data not shown), which made the powder stickier.

Table 3. Carr's index of ITZ liquisolid systems and physical mixtures.

Formula	Carr's index (%)
DCT-PM	23.44 ± 1.12
LS-LC	17.58 ± 0.89
LS-PVP-0%	18.00 ± 0.75
LS-PVP-0.5%	17.94 ± 0.52
LS-PVP-1%	17.88 ± 0.61
LS-PVP-5%	16.66 ± 0.55
LS-PVP-10%	15.60 ± 0.42
LS-PVP-20%	23.21 ± 0.98

3.4.2. Differential Scanning Calorimetry (DSC)

DSC is one useful technique to study possible physicochemical interaction between drug entity and the excipients in a formulation. Fig. (**3**) showed thermal behaviour of pure ITZ, Neusilin® US2, PVP, physical mixtures and liquisolid systems. The thermogram of pure ITZ revealed a sharp endothermic peak at 166.2 °C corresponding to its melting temperature. Such sharp endothermic peak indicated that was in pure crystalline state. The thermograms of Neusilin® US2 and PVP displayed broad endothermic peaks around 80 °C and 222 °C, respectively. The thermogram of DCT-PM formulation showed the same sharp characteristic endothermic peak around 166 °C with reduced intensity, indicating that there were no changes in crystallinity of the drug or no interaction between drug and exipients in the conventional formulation. Whereas, for liquisolid formulation LS-LC, LS-PVP-1% and LS-PVP-5%, the characteristic melting peak of ITZ was disappeared, indicating that the drug was solubilized and molecularly dispersed with excipients within the liquisolid matrix led to formation of an amorphous solid solution [16, 39-40]. The thermogram of liquisolid formulations LS-PVP-0% showed a small broadened peak with markedly reduced intensity at about 166 °C. This signified both drug melting point and crystallinity reduced due to crystallization of ITZ in the liquid vehicle [41].

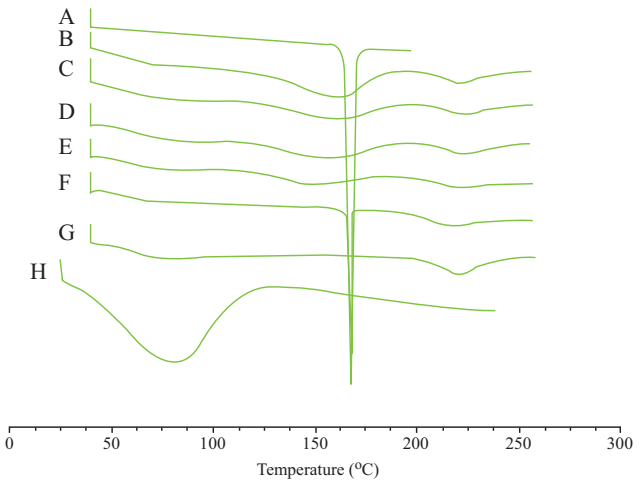

Fig. (3). Differential scanning calorimetric thermograms of (**A**) pure ITZ, liquisolid formulations (**B**) LS-PVP-0%, (**C**) LS-LC, (**D**) LS-PVP-1%, (**E**) LS-PVP-5%, (**F**) physical mixtures DCT-PM, (**G**) Neusilin® US2 and (H) PVP K30.

3.4.3. X-ray Powder Diffraction (XRPD)

The X-ray powder diffraction (XRPD) results (Fig. **4**) were in good agreement with the DSC. X-ray diffractogram of pure ITZ showed sharp distinct peaks supporting crystalline nature of drug. The physical mixture formulations had the same diffraction patterns, demonstrating that drug crystalline structure remained unchanged during the formulation process. However, the liquisolid powder X-ray diffraction pattern of LS-LC, LS-PVP-1% and LS-PVP-5% showed only one sharp diffraction peak belonging to Neusilin® US2, which maintained its crystalline state in liquisolid systems [16, 40]. Such an absence of ITZ constructive reflection in the liquisolid X-ray diffractogram indicated that ITZ had almost entirely converted from crystalline to amorphous or solubilised form [42]. But ITZ characteristic peaks were observed in liquisolid powder of formulation LS-PVP-0% due to few drug crystal particles within this system.

3.5. Evaluation of ITZ Liquisolid Formulations

3.5.1. Measurement of Contact Angle

The contact angle was related with the surface properties and wetting ability. In order to understand the mechanism of dissolution enhancement by liquisolid technique, contact angles of liquisolid compacts and conventional tablets were measured with 0.1 M hydrochloric acid solution as wetting fluid. As shown in Fig. (**5**), liquisolid compacts had smaller contact angles compared with conventional tablets, indicating better wettability. Moreover, the contact angle decreased as the amount of PVP increased. Because of the hydrophilic character and hygroscopicity of PVP, it could facilitate wetting of particles by decreasing interfacial tension between wetting fluid and tablet surface. Moreover, liquisolid compact LS-LC had the smallest contact angle. The proportion of

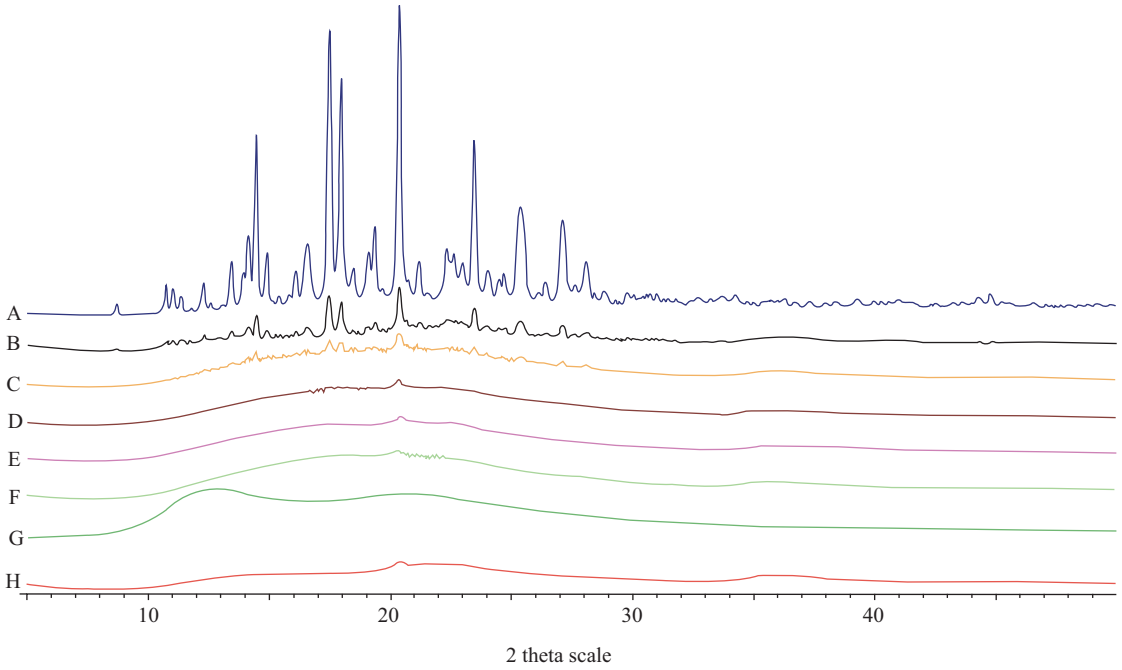

Fig. (4). X-ray powder diffractogram of (**A**) pure ITZ, (**B**) physical mixtures DCT-PM, liquisolid formulations (**C**) LS-PVP-0%, (**D**) LS-PVP-1%, (**E**) LS-PVP-5%, (**F**) LS-LC, (**G**) PVP K30 and (**H**) Neusilin® US2.

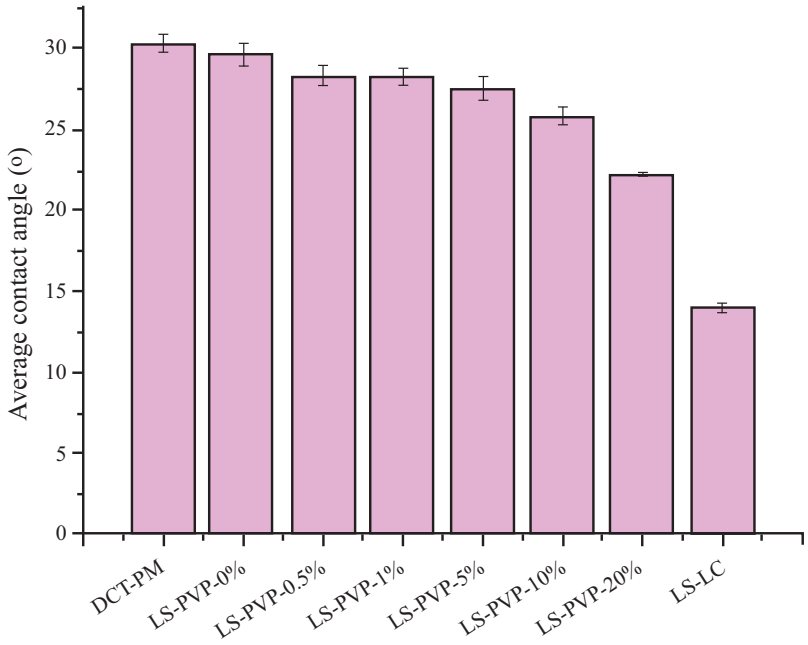

Fig. (5). Contact angle of liquisolid tablets and conventional tablets.

NMP in LS-LC was higher than other liquisolid compacts. NMP could interact with water molecules ensuring their complete miscibility by its polar disubstituted cyclic amide group [28].

3.5.2. Dissolution Studies

Fig. (**6**) illustrated the dissolution profiles of liquisolid tablets and conventional tablets. The dissolution of ITZ from all liquisolid tablets was higher than that from conventional tablets ($p < 0.05$). The percentages of ITZ dissolved at 30 min of LS-LC, LS-PVP-0.5% and LS-PVP-1% were more than 85%, whereas the percentage of ITZ dissolved at 30 min of conventional tablets was only 15.19%. In order to have a better comparison of the extent and the rate of drug dissolved, $Q_{5\ min}$ (percent drug dissolved within 5 min) and $T_{50\%}$ (time required for the dissolution of 50% drug) were calculated (Table **4**). The results clearly affirmed that all liquisolid tablets had higher $Q_{5\ min}$ and shorter $T_{50\%}$ (except LS-PVP-20%) compared to DCT-PM ($p < 0.05$).

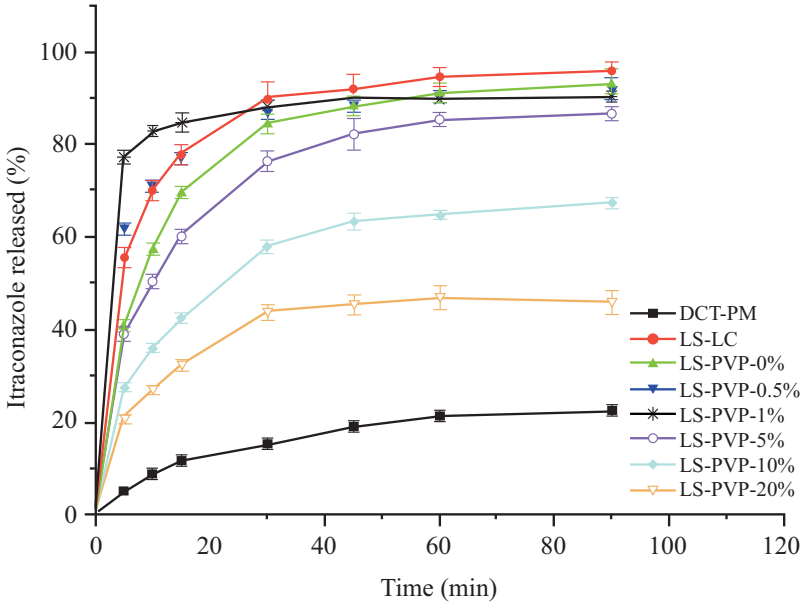

Fig. (6). Dissolution profiles of ITZ from the liquisolid tablet systems and the conventional tablets.

Table 4. Release parameters of liquisolid and conventional formulations.

Formula	$Q_{5\ min}$ (%)	$T_{50\%}$ (min)
DCT-PM	5.16 ± 1.24	> 90
LS-LC	55.57 ± 3.89	4.30 ± 0.42
LS-PVP-0%	40.76 ± 3.54	7.30 ± 0.84
LS-PVP-0.5%	61.78 ± 4.31	4.75 ± 0.57
LS-PVP-1%	77.35 ± 3.89	3.00 ± 0.32
LS-PVP-5%	39.06 ± 3.15	9.75 ± 1.08
LS-PVP-10%	27.44 ± 2.36	21.51 ± 3.52
LS-PVP-20%	20.72 ± 3.11	> 90

$Q_{5\ min}$: percent drug dissolved within 5 min; $T_{50\%}$: time required for the dissolution of 50% drug.

In the liquisolid systems, ITZ was almost or completely solubilized and molecularly dispersed within a water-miscible liquid vehicle. Drug release from liquisolid compacts was solely dependent on the disintegration of the tablets and the miscibility of the liquid portion with the dissolution medium [43]. Therefore, due to the significantly increased wetting properties and surface area of the drug particles available for dissolution, liquisolid tablets were expected to enhance drug dissolution [16, 30, 40-41, 44]. Whereas, for conventional tablets, the surface area available for dissolution was very limited due to the hydrophobic properties of ITZ. According to the results of DSC, XRPD and contact angle, it could be concluded that increased dissolubility, wetting properties and surface area available for dissolution contributed to the improvement of the dissolution of ITZ from liquisolid tablets.

To learn more about the drug release mechanism, the drug release profiles were fitted in four release models as follows: Zero order kinetics, First order kinetics, Higuchi [45], and Korsmeyer-Peppas [46]. As shown in Table 5, the release of ITZ from liquisolid tablets was best fitted for Korsmeyer-Peppas model according to the correlation coefficient (R^2). The value of n in Korsmeyer-Peppas equation ($F = kt^n$, F was the drug released fraction at time t, k was a constant and n was the release exponent) was lower than 0.43, which indicated that the release of ITZ from liquisolid tablets was based on Fick's law of diffusion. This meant that the drug concentration gradient between the tablet and the bulk of the dissolution medium serves as a driving force for diffusion of drug molecules from the tablet into the dissolution medium, hence driving drug dissolution. Therefore, the molecularly dispersed state of ITZ in liquid vehicles increased drug saturation solubility, hence leading to increase in overall concentration gradient, which ultimately facilitated the release of ITZ from liquisolid tablets [16, 44].

As shown in Fig. (**6**), the amount of PVP in the liquid portion had an effect on drug release from liquisolid compacts. The $Q_{5\ min}$ of LS-PVP-0%、LS-PVP-0.5% and LS-PVP-1% were 40.76 ± 3.54%, 61.78 ± 4.31% and 77.35 ± 3.89%, respectively. This signified that the presence of low amount of PVP in liquisolid formulation could enhance disintegration and dissolution of ITZ liquisolid tablets. PVP could act as a disintegrating agent in liquisolid tablets due to its hydrophilic character and hygroscopicity. Meanwhile PVP could increase the wettability of liquisolid tablet as mentioned above. Importantly, PVP may inhibit precipitation of drug from the supersaturated solution and increase the amount of molecularly dispersed drug, and hence, the surface area of drug exposed to the dissolution medium was increased [19, 33]. However, the percentage of PVP over 5% decreased the dissolution of ITZ from liquisolid tablets. As more PVP was incorporated in liquisolid formulation, more reduction in drug release rate was observed. The amount of PVP below 1% would not significantly increase the viscosity

Table 5. Drug release kinetic parameters of liquisolid formulations.

Formula	Zero order	First order	Higuchi	Korsmeyer-Peppas	
	R^2	R^2	R^2	R^2	n
LS-LC	0.6820	0.8901	0.8271	0.9162	0.186
LS-PVP-0%	0.6933	0.8735	0.8373	0.9099	0.282
LS-PVP-0.5%	0.7148	0.8453	0.8552	0.9456	0.140
LS-PVP-1%	0.6632	0.7415	0.8112	0.9273	0.053
LS-PVP-5%	0.7548	0.8639	0.8872	0.9524	0.289
LS-PVP-10%	0.7764	0.8314	0.9014	0.9593	0.327
LS-PVP-20%	0.6756	0.6928	0.8243	0.9201	0.296

of the drug-vehicle mixture, whereas the viscosity of the drug-vehicle mixture enormously increased as the amount of PVP increased over 5% (data not shown). Hence, the viscosity and thickness of the stagnant diffusion layer between drug particle and the dissolving fluid would significantly increase as the amount of PVP increased, subsequently, the release of ITZ from liquisolid tablets was retarded [18]. Therefore PVP may have a dual effect on the dissolution of ITZ from liquisolid tablets. A small amount of PVP could enhance dissolution of ITZ from liquisolid tablets, whereas large amount of PVP retarded drug release.

4. CONCLUSION

High amount of ITZ was loaded into liquisolid compact by using NMP as liquid vehicle, Neusilin® US2 as carrier/coating material and PVP as a precipitation inhibitor. All the liquisolid tablets showed higher drug dissolution rates compared with the conventional tablets. Importantly, PVP added into liquid medication showed enhancement effect on stability of liquid medication, flowability of liquisolid powders and wetting ability of liquisolid tablets. PVP may have a dual effect on the dissolution of ITZ from liquisolid tablets. A small amount of PVP could enhance dissolution of ITZ from liquisolid tablets, whereas large amount of PVP retarded drug release.

CONFLICT OF INTEREST

The authors declared that this article content has no conflict of interest.

ACKNOWLEDGEMENTS

This study was supported by the National Key Technologies R&D Program for New Drugs (Grant No. 2012ZX09-301003-001-009).

PATIENT CONSENT

Declared none.

REFERENCES

[1] Rinaki, E.; Valsami, G.; Macheras, P. Quantitative biopharmaceutics classification system: the central role of dose/solubility ratio. *Pharm. Res*., **2003**, *20*, 1917-1925.

[2] Vasconcelos, T.; Sarmento, B.; Costa P. Solid dispersions as strategy to improve oral bioavailability of poor water soluble drugs. *Drug Discov. Today*, **2007**, *12*, 1068-1075.

[3] Van Hoogevest, P.; Liu, X.; Fahr, A. Drug delivery strategies for poorly watersoluble drugs: the industrial perspective. *Expert Opin. Drug Deliv*., **2011**, *8*, 1481-1500.

[4] Beule, K.D.; Gestel, J.V. Pharmacology of itraconazole. *Drugs*, **2001**, *61*, 27-37.

[5] Peeters, J.; Neeskens, P.; Tollenaere, J.P.; Van Remoortere, P.; Brewster, M.E. Characterization of the interaction of 2-hydroxypropyl-beta-cyclodextrin with itraconazole at pH 2, 4 and 7. *J. Pharm. Sci.*, **2002**, *91*, 1414-1422.

[6] Van Eerdenbrugh, B.; Van Speybroeck, M.; Mols, R.; Houthoofd, K.; Martensb, J.A.; Froyenc, L.; Van Humbeeckc, J.; Augustijnsa, P.; Van den Mootera, G. Itraconazole/TPGS/Aerosil®200 solid dispersions Characterization, physical stability and *in vivo* performance. *Eur. J. Pharm. Sci.*, **2009**, *38*, 270-278.

[7] Kumar, S.; Shen, J.; Burgess, D.J. Nano-amorphous spray dried powder to improve oral bioavailability of itraconazole. *J. Control. Release*, **2014**, *192*, 95-102.

[8] Kim, J.K.; Park, J.S.; Kim, C.K. Development of a binary lipid nanoparticles formulation of itraconazole for parenteral administration and controlled release. *Int. J. Pharm.*, **2010**, *383*, 209-215.

[9] Cerdeira, A.M.; Mazzotti, M.; Gander, B. Formulation and drying of miconazole and itraconazole nanosuspensions. *Int. J. Pharm.*, **2013**, *443*, 209-220.

[10] Kucuk, I.; Ahmad, Z.; Edirisinghe, M.; Orlu-Gul, M. Utilization of microfluidic V-junction device to prepare surface itraconazole adsorbed nanospheres. *Int. J. Pharm.*, **2014**, *472*, 339-346.

[11] Zheng, W.S.; Fang, X.Q.; Wang, L.L.; Zhang, Y.J. Preparation and quality assessment of itraconazole transfersomes. *Int. J. Pharm.*, **2012**, *436*, 291-298.

[12] Curić, A.; Reul, R.; Möschwitzer, J.; Fricker, G. Formulation optimization of itraconazole loaded PEGylated liposomes for parenteral administration by using design of experiments. *Int. J. Pharm.*, **2013**, *448*, 189-197.

[13] Akkar, A.; Müller, R.H. Intravenous itraconazole emulsions produced by SolEmuls technology. *Eur. J. Pharm. Biopharm.*, **2003**, *56*, 29-36.

[14] Yi, Y.; Yoon, H.J.; Kim, B.O.; Shim, M.; Kim, S.O.; Hwang, S.J.; Seo, M.H. A mixed polymeric micellar formulation of itraconazole: characteristics, toxicity and pharmacokinetics. *J. Control. Release*, **2007**, *117*, 59-67.

[15] Nokhodchi, A.; Javadzadeh, Y.; Siahi-Shadbad, M.R.; Barzegar-Jalali, M. The effect of type and on the dissolution rate of a poorly soluble drug (indomethacin) from liquisolid compacts. *J. Pharm. Pharma. Sci.*, **2005**, *8*, 18-25.

[16] Fahmy, R.H.; Kassem, M.A. Enhancement of famotidine dissolution rate through liquisolid tablets formulation: *In vitro* and *in vivo* evaluation. *Eur. J. Pharm. Biopharm.*, **2008**, *69*, 993-1003.

[17] Tiong, N.; Elkordy, A.A. Effects of liquisolid formulations on dissolution of naproxen. *Eur. J. Pharm. Biopharm.*, **2009**, *73*, 373-384.

[18] Nokhodchi, A.; Aliakbar, R.; Desai, S.; Javadzadeh, Y. Liquisolid compacts: the effect of cosolvent and HPMC on theophylline release. *Colloids Surf. B Biointerfaces*, **2010**, *79*, 262-269.

[19] Javadzadeh, Y.; Siahi, M.R.; Asnaashari, S.; Nokhodchi, A. An investigation of physicochemical properties of piroxicam liquisolid compacts. *Pharm. Dev. Technol.*, **2007**, *12*, 337-343.

[20] Yadav, V.B.; Yadav, A.V. Improvement of solubility and dissolution of indomethacin by liquisolid and compaction granulation technique. *J. Pharm. Sci. Res.*, **2009**, *1*, 44-51.

[21] Syed, I.A.; Pavani, E. The liquisolid technique: based drug delivery system. *Int. J. Pharm. Sci. Drug Res.*, **2012**, *4*, 88-96.

[22] Hentzschel, C.M.; Sakmann, A.; Leopold, C.S. Suitability of various excipients as carrier a nd coating materials for liquisolid compacts. *Drug. Dev. Ind. Pharm.*, **2011**, *37*, 1200-1207.

[23] Raghavan, S.L.; Trividic, A.; Davis, A.F.; Hadgraft, J. Effects of cellulose polymers on supersaturation and *in vitro* membrane transport of hydrocortisone acetate. *Int. J. Pharm.*, **2000**, *193*, 231-237.

[24] Raghavan, S.L.; Trividic, A.; Davis, A.F.; Hadgraft, J. Crystallization of hydrocortisone acetate: influence of polymers. *Int. J. Pharm.*, **2001**, *212*, 213-221.

[25] Akinlade, B.; Elkordy, A.A.; Essa, E.A.; Elhagar, S. Liquisolid systems to improve the dissolution of furosemide. *Sci. Pharm.*, **2010**, *78*, 325-344.

[26] Spireas, S. Liquisolid systems and methods of preparing same. U.S. Patent 6,423,339, July, 23, 2002.

[27] Carr, R.L. Evaluation flow properties of solids. *Chem. Eng.*, **1965**, *72*, 163-168.

[28] Sanghvi, R.; Narazaki, R.; Machatha, S.G.; Yalkowsky, S.H. Solubility improvement of drugs using N-methyl pyrrolidone. *AAPS Pharm. SciTech.*, **2008**, *9*, 366-376.

[29] Jouyban, A.; Fakhree, M.A.; Shayanfar, A. Review of pharmaceutical applications of N-methyl-2-pyrrolidone. *J. Pharm. Pharm. Sci.*, **2010**, *13*, 524-535.

[30] Naveen, C.; Shastri. N.; Tadikonda. R.R. Use of the liquisolid compact technique for improvement of the dissolution rate of valsartan. *Acta Pharm. Sin. B.*, **2012**, *2*, 502-508.

[31] Javadzadeh, Y.; Musaalrezaei, L.; Nokhodchi, A. Liquisolid technique as a new approach to sustain propranolol hydrochloride release from tablet matrices. *Int. J. Pharm.*, **2008**, *362*, 102-108.

[32] Xu, S.; Dai W.G. Drug precipitation inhibitors in supersaturable formulations. *Int. J. Pharm.*, **2013**, *453*, 36-43.

[33] Brouwers, J.; Brewster, M.E.; Augustijns, P. Supersaturating drug delivery systems: the answer to solubility-limited oral bioavailability? *J. Pharm. Sci.*, **2009**, *98*, 2549-2572.

[34] Warren, D.B.; Benameur, H.; Porter, C.J.; Pouton, C.W. Using polymeric precipitation inhibitors to improve the absorption of poorly water-soluble drugs: a mechanistic basis for utility. *J. Drug Target*, **2010**, *18*, 704-731.

[35] Xie, S.; Poornachary, S.K.; Chow, P.S.; Tan, R.B.H. Direct precipitation of micronsize salbutamol sulfate: new insights into the action of surfactants and polymeric additives. *Cryst. Growth Des.*, **2010**, *10*, 3363-3371.

[36] Chen, Y.; Liu, C.; Chen, Z.; Su, C.; Hageman, M.; Hussain, M.; Haskell, R.; Stefanski, K.; Qian, F. Drug-polymer-water interaction and its implication for the dissolution performance of amorphous solid dispersions. *Mol. Pharm.*, **2015**, *12*, 576-589.

[37] Nguyen, D.N.; Van den Mooter, G. The fate of ritonavir in the presence of darunavir. *Int. J. Pharm.*, **2014**, *475*, 214-226.

[38] Lindfors, L.; Forssén, S.; Westergren, J.; Olsson, U. Nucleation and crystal growth in supersaturated solutions of a model drug. *J. Colloid Interface Sci.*, **2008**, *325*, 404-413.

[39] Mura, P.; Faucci, M.T.; Parrini, P.L. Effect of grinding with microcrystalline cellulose and cyclodextrins on the ketoprofen physicochemical properties. *Drug Dev. Ind. Pharm.*, **2001**, *27*, 119-128.

[40] Sayyad, F.J.; Tulsankar, S.L.; Kolap, U.B. Design and development of liquisolid compact of candesartan cilexetil to enhance dissolution. *J. Pharm. Res.*, **2013**, *7*, 381-388.

[41] Elkordy, A.A.; Essa, E.A.; Dhuppada, S.; Jammigumpulaa, P. Liquisolid technique to enhance and to sustain griseofulvin dissolution: effect of choice of non-volatile liquid vehicles. *Int. J. Pharm.*, **2012**, *434*, 122-132.

[42] Kapure, V.J.; Pande, V.V.; Deshmukh, P.K. Dissolution enhancement of rosuvastatin calcium by liquisolid compact technique. *J. Pharm.*, **2013**, *2013*, 1-9.

[43] Hentzschel, C.M.; Alnaief, M.; Smirnova, I.; Sakmann, A.; Leopold, C.S. Enhancement of griseofulvin release from liquisolid compacts. *Eur. J. Pharm. Biopharm.*, **2012**, *80*, 130-135.

[44] Elkordy, A.A.; Tan, X.N.; Essa, E.A. Spironolactone release from liquisolid formulations prepared with Capryol™ 90, Solutol® HS-15 and Kollicoat® SR 30 D as non-volatile liquid vehicles. *Eur. J. Pharm. Biopharm.*, **2013**, *83*, 203-223.

[45] Higuchi, T. Mechanism of sustained-action medication. Theoretical analysis of rate of release of solid drugs dispersed in solid matrices. *J. Pharm. Sci.*, **1963**, *52*, 1145-1149.

[46] Korsmeyer, R.W.; Peppas, N.A. Effect of the morphology of hydrophilic polymeric matrices on the diffusion and release of water soluble drugs. *J. Membr. Sci.*, **1981**, *9*, 211-227.

Soft Tissues and Materials

JOURNAL OF
biomaterials applications

Journal of Biomaterials Applications
2018, Vol. 32(7) 920–931

DOI: 10.1177/0885328217744080
journals.sagepub.com/home/jba
SAGE

Immune response of bovine sourced cross-linked collagen sponge for hemostasis

Lin Zhang[1], Xufeng Niu[1], Lei Sun[1], Zhending She[2], Rongwei Tan[2] and Wei Wang[3]

Abstract

A comprehensive immunogenicity scheme is proposed to examine immune response of bovine sourced hemostasis collagen sponge to establish foundation for further researches and decrease the incidence of adverse reaction in clinical trials. Compared with negative control group without any implant, spleen and lymph nodes morphology show no apparent swelling in mice with different doses of collagen sponge implants. Immune cells population, especially lymph nodes cells population, is practically coincident with organs. However, splenic cells display slight proliferation in early phase following collagen sponge implantation. Splenic cells apoptosis also demonstrates no significant difference among all groups. T lymphocytes subsets, CD4/CD8 cells ratio, in spleen and lymph nodes are practically normal. Splenic cells Ki67 + proportions do not exhibit significant difference between collagen sponge groups and negative control group. Humoral response is determined by detection of IgG and IgM concentration in serum, not exhibiting remarkable increase with collagen sponge implantation, compared to the drastic increase in positive control group with bovine tendon implantation. Local analysis around implants by hematoxylin-eosin staining discovers slight cell infiltration around collagen sponge. Tumour necrosis factor-α immunostaining indicates slight inflammation in early phase following collagen sponge implantation, but interferon-γ immunostaining is negligible even in positive control group. Collagen sponge, especially in high dose, may have evoked benign immune response in BALB/c mice, but this response is transient. The present evaluation scheme for immune response is integrated and comprehensive, suitable for various biomaterials.

Keywords

Immune response, collagen, in vivo, lymphocytes, inflammation

Introduction

Collagen has received extensive attention in recent years and been fabricated for a variety of medical applications, such as bone regeneration,[1–5] periodontal regeneration,[6] vascular repair,[7] tracheoesophageal fistula repair,[8] skin repair,[9–12] corneal scaffold, drug release,[13] etc. A number of these products are FDA-approved for human use. It should be informed that hemostat is another conventional application of collagen.[14–16] It is a kind of effective hemostat, which is involved in platelet adhesion, aggregation and activation, as well as modulating thrombin formation to boost coagulation.[17] Collagen is applied to many bleeding surgeries with high risks, like cardiac operations,[18] gynecological and obstetric, neurosurgical surgeries, and it has been proved to significantly reduce blood-loss and decrease hemorrhage duration in an anticoagulated swine model,[14] as well as in clinical cardiac surgery.[18]

Notoriously, collagen is typical of low immunogenicity. However, this characteristic is possessed by pure collagen. For most collagen-based products, collagen

[1]Key Laboratory for Biomechanics and Mechanobiology of Ministry of Education, School of Biological Science and Medical Engineering, Beihang University, Beijing, P. R. China
[2]Shenzhen Lando Biomaterials Co., Ltd, Shenzhen, P. R. China
[3]Department of Immunology, School of Basic Medical Sciences, Peking University, Key Laboratory of Medical Immunology, Ministry of Health (Peking University), Beijing, P. R. China

Corresponding author:
Wei Wang, Department of Immunology, School of Basic Medical Sciences, Peking University, Beijing 100191, P. R. China.
Email: wangwei83427@bjmu.edu.cn

component is extracted from animals. Animal proteins, DNA or RNA, and cells inevitably remain in objective collagen. The previous researches demonstrated that structure of collagen,[19] the presence of cells and noncollagenous protein,[20,21] crosslinking treatments[22] would alter the immunogenicity of collagen and evoke immune response. In addition, some studies also showed that noncollagenous protein contaminants, which were proved to be main immunogenic components of collagen hemostats,[21,23] contributed to adverse reactions in clinic. Since immunogenicity is the primary cause of immunotoxicity, the immunogenicity evaluation is critical and urgent for collagen products.

In the previous studies, antibody detection by enzyme-linked immunosorbent assay (ELISA) and histology analysis by hematoxylin-eosin (H&E) staining for cell infiltration were the most frequently utilized methods to access immune response.[22,24–26] However, the more thorough and comprehensive estimation of immune response was quite rare. This study proposes an evaluation scheme for immune response elicited by a new kind of hemostatic collagen sponge (CS) derived from bovine tendon (BT). Multiple doses and harvesting time points are set to assess the impact of collagen dose on immune response and the duration of immune response.

The scheme is designed from immune organ, immune tissue, immune cell and immune molecule, to comprehensively estimate the immunogenicity of this CS. Functional and non-functional tests are also included in this plan. In addition, systematic and local, humoral and cellular immune responses are all evaluated by these varied tests. Immune organs, immune cells population, proliferation, apoptosis and phenotype are performed to access systematic immune response. Humoral response intensity is judged by antibody concentration in serum. Cellular and local response is evaluated by observing cell infiltration and inflammation-related cytokines expression.

Materials and methods

Materials and animals

The experimental procedures had been approved by the ethics committee of Peking University Health Science Centre. The animal group consisted of 100 female BALB/c mice, aged six-to-eight-week-old and weighing 18–22 g, five mice for per group per time point. Mice in negative control (NC) group underwent surgeries but no implants. Mice in three experimental groups and positive control (PC) group were implanted high, moderate, low dose of sterile CS (CS-H, CS-M, CS-L), and BT (from which CS-H can be extracted), respectively. Sterilized CS, supplied by Shenzhen Lando Biomaterials Co., Ltd, was cut into pieces of $8.6 \times 8.7\,mm^2$ as CS-H, $4.3 \times 8.7\,mm^2$ as CS-M and $4.3 \times 4.35\,mm^2$ as CS-L under sterile conditions before surgeries. CS-L is calculated based on the maximum dose on human per time determined by manufacturer and surface area ratio of human and mice. As mice have higher tolerance than human, we also set higher doses, namely CS-M and CS-H.

Surgeries

Animals were anesthetized by 0.5% sodium pentobarbital, and dorsal skins were disinfected with 75% alcohol. A 1.5 cm incision was made and 1 subcutaneous pocket was produced by scissors, then 1 piece of material (for PC or CS groups) was inserted into the pocket. Polyglycolic acid suture with needle was employed to sew up the incision. Three implantations at three dorsum sites were performed to immunize mice at one-week interval. After three immunizations, mice were respectively raised for 7, 14, 30, 60 days and then sacrificed for post-implantation study. At every harvesting time point, 1 eyeball of each mouse was picked out for blood, which was collected in a 1.5 mL EP tube, and then the mouse was euthanized by cervical dislocation. In addition, the animal group for seven-day study was selected and cut tails to collect blood on day 3 post-implantation for antibody analysis. Following cervical dislocation, under strict aseptic conditions, abdominal skin was sheared. Lymph nodes at two armpits and one groin close to incision were picked out and immersed in sterile phosphate buffer solution (PBS). The abdomen was opened and the spleen was also plucked and immersed in sterile PBS. Skin biopsies together with implants were dissected out and fixed in 4% paraformaldehyde for histological analysis. After every tube of blood was layered, serum and blood cells were separated by centrifugation, and sera were stored at $-20\,^{\circ}C$ until analysis. Lymph nodes of PC, NC and CS-H or CS-M or CS-L were neatly put together to be photographed. Following that, lymph nodes were ground with needle bar and 40 μm cell strainers to obtain cell suspension under strict aseptic conditions. Spleens were dealt with the same way as lymph nodes.

Cell counting

Spleen cells need to be disposed of erythrocytes before counting. In detail, spleen cells were collected by centrifugation, then supernatant was discarded and red blood cell lysis buffer was added to split erythrocytes. After splitting, splenic mononuclear cells were collected by another centrifugation and constant volume PBS was added to suspend cells. The obtained cells were

counted by automatic blood cell counter. Lymph node cells were washed and counted directly.

Splenic cell proliferation

Flat-bottom micro-titre 96-well plates and Cell Counting Kit (CCK8) were used for splenic cell proliferation. About 2×10^5 cells were suspended in 200 μL RPMI-1640 complete culture medium (containing 10% fetal bovine serum and 1% penicillin-streptomycin) and added to each well. Phorbol-12-myristate-13-acetate (PMA) and ionomycin (Iono) were also added in 200 μL medium by 100 ng/mL and 1000 ng/mL to boost cell proliferation in vitro. The plates were then incubated in 37 °C , 5% CO_2 incubator for three days. After removing the upper solution carefully, 100 μL of the mixture of 10% CCK8 and 90% RPMI-1640 complete culture medium was added in each well. About 1 h later, the solution in each well was mixed and absorbance was measured at 450 nm.

Splenic cell apoptosis

Cells were incubated with PMA and Iono as the same way with proliferation assay. Annexin-v-FLUOS and 7-Amino-Actinomycin D (7AAD) were employed to analyse splenic cell apoptosis. The following steps were conducted under the manufacturer specifications. Annexin-v-FLUOS, 7AAD and HEPES buffer were mixed by a ratio in advance. After being washed by PBS, the cells were incubated with the above-mentioned solution in the dark at room temperature for 30 min. The samples were analysed with a FACS Canto II.

Cell phenotype and flow cytometry

Five fluorochrome-conjugated monoclonal antibodies specific for murine CD19 (PE-Cy7), TCR (APC), CD4 (FITC), CD8 (PerCP), Ki67 (PE) were purchased from BD Biosciences for phenotype identification and cell sorting in splenic cells and lymph node cells. Unspecific cell surface-binding was blocked by Fc-Block on ice for 30 min, and then all immunofluorescence staining was performed by incubating cells with diluted antibodies,[27–29] as recommended by the manufacturer. All samples were then processed with an FACS Canto II cytometer. The cells were sorted with FACS Aria Cell Sorter and the data were analysed with Flow Jo software. Anti-CD19 PE-Cy7, anti-TCR APC were foremost used to characterize T lymphocytes and B lymphocytes, then two T lymphocytes subsets, CD4 + and CD8 + cells were identified by anti-CD4 FITC and anti-CD8 PerCP staining. Anti-Ki67 PE was applied for the identification of proliferating cells.

ELISA

Flat-bottom micro-titre 96-well plates specific for ELISA were utilized to IgM and IgG concentration detection in serum. The purified rat anti-mouse IgM antibody and mouse IgM isotype control were obtained from BD Biosciences. Goat anti-mouse IgG (Fc specific)-peroxidase antibody and goat anti-IgM (μ-chain specific)-peroxidase antibody were supplied by Sigma. Goat anti-mouse IgG was obtained from Merck Millipore. Mouse IgG isotype control was purchased from Invitrogen. This study adopted standard ''sandwich'' ELISA. All wells were washed with PBST (PBS containing 0.05% tween-20) and then fully dried before being adding another solution. The micro-titre wells were coated with coating antibody solution at 4 °C overnight. After washing the wells from excess antibodies for three times, PBSB (PBS containing 1% bovine serum albumin) was added to each well to block these non-specific bindings. Serial double dilutions of sera taken from naive mice and 10^5 (IgG)/10^4 (IgM) dilutions of sera from specifically immunized mice were added to the wells. After being washed from excess sera, the plates were added diluted peroxidase-labelled goat anti-mouse IgG/IgM (diluted in PBSB by 1: 1000) and incubated. The substrate, 3, 3′, 5, 5′-tetramethylbenzidine, was added to these rinsed wells to induce a colour reaction. The absorbance was read at 450 nm after stopping the reaction by the addition of 2 M sulphuric acid (H_2SO_4) solution.

Histological analysis

As previously described,[30,31] after fixation in 4% paraformaldehyde, the skin samples were washed with running water, dehydrated overnight in a tissue processor, and embedded in paraffin. The paraffin blocks were cut into 3–5 μm sections and mounted on glass slides, then deparaffinized and stained with H&E as standard procedures for optical microscopy to assess total cell infiltration.

Immunohistochemistry analysis

For immunostaining, paraffin sections were deparaffinized and subjected to immunohistochemistry staining with antibodies, including anti-tumour necrosis factor-α (TNF-α) and anti-interferon-γ (IFN-γ). Steps were standard and followed the previous descriptions in literatures.[32,33] In detail, sections to be stained were rehydrated, underwent antigen retrieval, quenched endogenous tissue peroxidases and blocked. Subsequently, all sections were incubated with the primary antibody and biotinylated secondary antibody and then incubated with avidin and biotinylated

horseradish peroxidase after washing. The substrate, 3, 3′-diaminobenzidine, was added to induce a colour reaction and then hematoxylin was added to counterstain. After being dehydrated, permeabilized and mounted, the slides were visualized on an optical microscope.

Statistical analysis

All charts and graphs were exported from GraphPad Prism Version 6. Statistical analysis was performed in IBM SPSS Statistics Version 22. Data are expressed as mean ± standard deviation (SD) of at least three animals for per group per time point and analysed by one-way ANOVA with LSD post-test for multiple comparisons. Difference is regarded as statistically significant when $p < 0.05$*, $p < 0.01$**, $p < 0.005$*** compared to NC.

Results

Immune organs and cell population

Spleens and lymph nodes of CS, NC and PC groups were captured for morphology comparison at every time point, as shown in Figure 1. It is apparent that spleens of CS groups do not show remarkable size differences from those of NC group, while PC group is macroscopically characterized by splenomegaly, significantly bigger than NC group at any time points (Figure 1(a)). Results of lymph nodes are practically consistent with those of spleens (Figure 1(c)). Lymph nodes in mice with BT implants are also noticeably chubbier than those of other groups, and lymph nodes in mice with CS implants do not exhibit obvious expansion. From these images, we can make a probable conclusion that immune response occurred in CS implanted mice is weak.

To prove the preliminary conclusion that the swelling of spleens and lymph nodes is associated with immune cell proliferation simulated by implants, cell counting was conducted. Figure 1(b) and (d) summarize the results. As illustrated in Figure 1(b), the number of splenic immune cells in CS groups is comparable to that in NC group, all fluctuating at approximately 1×10^8. Noticeably, these cell numbers are always lower than those of PC group, implanted BT, over 2.5×10^8. Another finding is that the splenic cell numbers of CS-H group are slightly higher than those of CS-L at day 14, 30, 60 post-implantation, whereas the

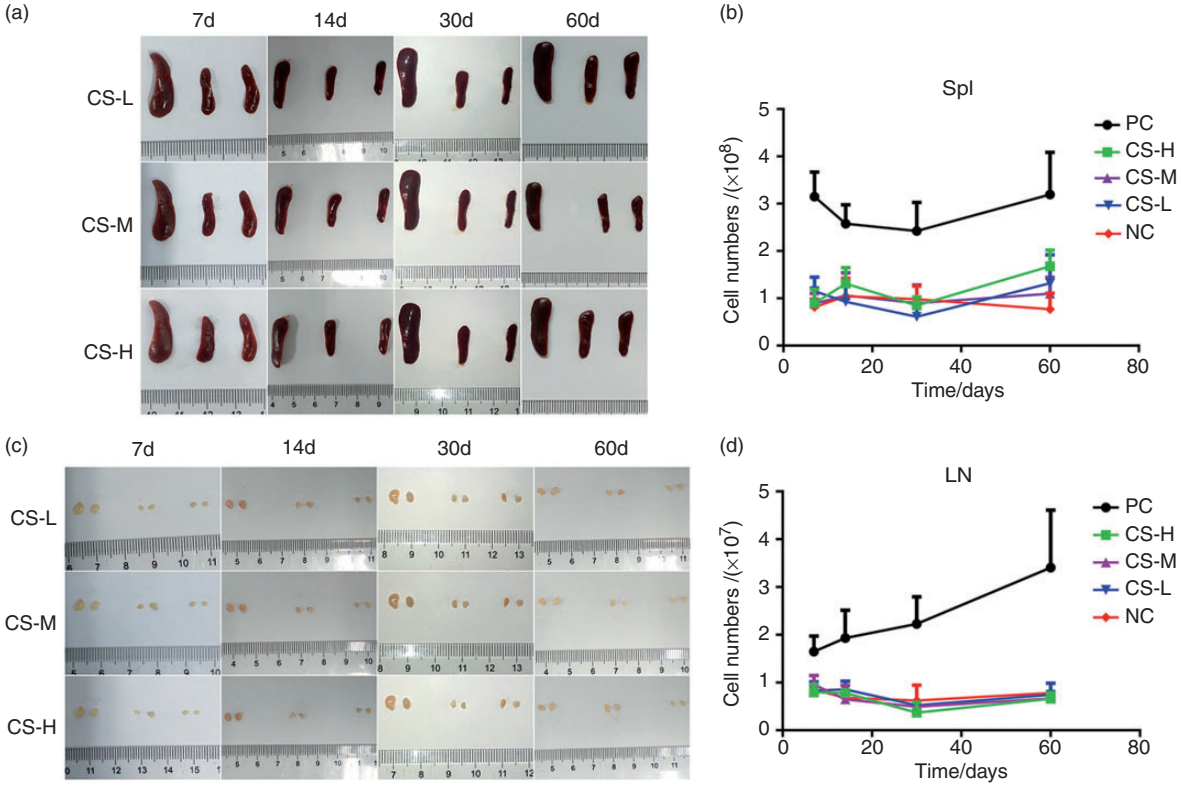

Figure 1. Representative images of spleens (a) and lymph nodes (c) at different time points. In every image, they are put from left to right in order of PC, CS and NC. Immune cell population of spleens (b) and lymph nodes (d).
Spl: spleen; LN: lymph nodes.

differences between CS-M and CS-L or CS-H are not distinct, which might imply that slightly more violent immune response has been initiated by CS-H than CS-L. Counting results of lymph nodes cells (Figure 1(d)) are more apparent, that is the other four groups are quite close to each other at any harvesting time points, ranging from about 0.6×10^7 to 1×10^7, while cell population of PC group is much greater, increasing continuously from approximately 2.6×10^7 to 3.2×10^7. Cell counting almost agrees to organ size differentiation determined by the unaided eye, so the swelling of spleens and lymph nodes of PC may be partially triggered by the increase of immune cell population. Splenic cell population difference between CS-H and CS-L indicates that higher dose of CS may have produced a greater stimulation and caused more cell proliferation. However, immune response induced by CS, even CS-H, is not so intense for analogous size of peripheral lymphoid organs and similar cell population to NC.

Splenic lymphocytes proliferation and apoptosis

Lymphocytes proliferation induced by mitogen in vitro is a means of assessing immune cell activation to grafts. In this study, PMA and Iono were applied to stimulate splenic lymphocytes to non-specifically proliferate in vitro. As seen in Figure 2(a) and (b), CS-H group displays significantly higher proliferation level than NC group in 14 days following implantation ($p < 0.001$, $p = 0.002$), but lymphocytes proliferative ability of CS-H group has dropped to the normal level by day 60 (Figure 2(c)). Mice in CS-M group and CS-L group fail to respond to implants by obvious lymphocytes proliferation, for the similar proliferation level to NC group at any time. Regarding CS dose effect on immune response, Figure 2 provides evidence that the absorbance of cell proliferation in CS-H group is approximately one-fold, even two-fold higher than those in CS-L and CS-M groups. The proliferation result at day 30 (data not shown) resembles to that at day 60. Overall, high-dose test material might have put a relatively benign stimulation on lymphocytes at the early time points in comparison to BT, while CS-M and CS-L do not produce obvious immune stimulation.

Immune cell apoptosis is critical in maintaining cellular balance and immune function. In this study, cell apoptosis primarily refers to activation induced cell apoptosis, and in theory, cell apoptosis degree can mirror cell activation level. Splenic lymphocytes apoptosis was also induced by PMA and Iono, but Figure 2(d) only illustrates the results at day 7, for the similarity of results at all time points. Although no significant apoptosis percentage differences are observed between NC group and other groups, CS-H group display slightly higher apoptosis percentage than

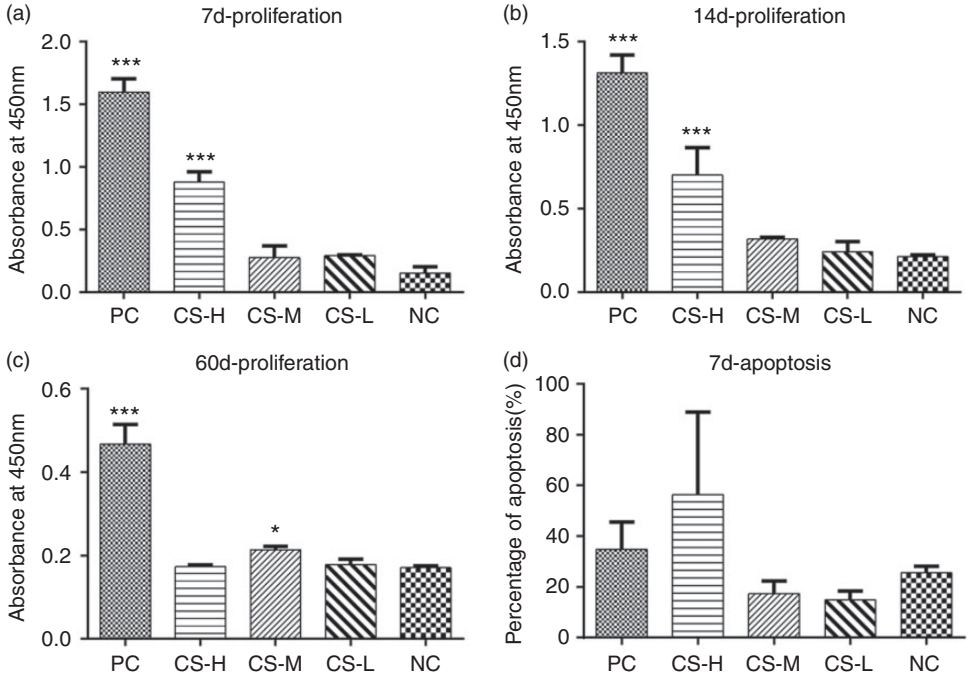

Figure 2. Splenic immune cells proliferation at day 7 (a), 14 (b), 60 (c) post-implantations, and splenic cells apoptosis at day 7 (d) in vitro under the stimulation of PMA and Iono.

NC group and other two CS groups, which indicates CS-H initiated more cell activation, in other words, CS-H may have produced a marginal stimulation to mice. Insufficient stimulants may account for the apoptosis proportion in PC group. In the following days, significant difference remains absent between CS groups and NC group (data not shown). Apoptosis results also indicate that CS is low immunogenic.

CD4/CD8 ratio

CD4 + and CD8 + T lymphocytes play a vital role in immune response and maintaining normal immune function. CD4/CD8 ratio is relatively invariable in normal state, despite of varied absolute numbers, so CD4+/CD8 + cell ratio is also an index of immune function evaluation and its variation can imply transplant rejection. In our study, percentages of CD4+, CD8 + and CD19 + lymphocytes were obtained by flow cytometry and displayed in flow cytometric plots (as shown in Supporting Information Figure S1), thereafter CD4/CD8 ratio was calculated (Figure 3). Significant difference of splenic CD4/CD8 ratio among all groups at every time point is almost absent, as all CD4+/CD8 + cell ratios are about 2, except the significant difference between CS-L and NC at day 14 (Figure 3(a)). In lymph nodes (Figure 3(b)), CD4/CD8 ratio varies from 2 to 3, but does not exhibit significant disparity among NC group and the others at day 7 and 30. However, CS-L and CS-M groups display fantastically higher CD4/CD8 ratio than NC group at day 14 ($p = 0.001$, 0.003), and PC group shows significantly lower ratio than NC group at day 60 ($p = 0.024$). From results of splenic CD4/CD8 ratio, we claim that CS does not trigger noticeable immune rejection, and not destroy immune function of mice as well, while implication of lymph nodes CD4/CD8 ratio remains to be discussed.

Ki67 expression

Ki67 is a signal antigen associated with cell proliferation, so Ki67 expression can represent lymphocytes activation level triggered by foreign antigen. Here, Ki67 immunostaining of splenic lymphocytes was applied to analyse the immunogenicity of CS (Representative flow cytometric plots are shown in Supporting Information Figure S2). According to Figure 4(a), CD4 + cells in NC and CS groups show approximately 10% Ki67 + percentage, except the abnormally higher percentage in NC group at day 7, which may be accounted for experimental errors. The difference between PC and CS groups lies in the increasing CD4+Ki67 + cell percentage of PC group, but steady CD4 + cell proliferation percentages of CS groups as NC group in the following days. Proliferation of CD8 + cells resembles to that of CD4 + cells (Figure 4(b)). CD8 + cells in NC and CS groups remain in relatively stable states and do not drastically proliferate all the time, with less than 10% activation proportion. In contrast, the disparity between PC and NC enlarges with time, up to day 60, about 40% CD8 + cells in PC group are in proliferative state, extremely significantly more than that in NC group, which is only 8% ($p = 0.002$). From proliferation of CD19 + cells (Figure 4(c)), we find that it displays about 20–30% proliferation percentage at day 14 although with no implant stimulation (Data at day 7 were not obtained for some reasons). CD19 + cells of PC group maintain that proliferation percentage at day 30 and 60, but other groups have declined to less than 20%, even 10% gradually. Thus, the significant difference arises between PC and NC group ($p = 0.001$), but no significant difference between CS and NC groups. These outcomes indicate that cell activation produced by CS implants is not noticeable, while implantation surgeries might have

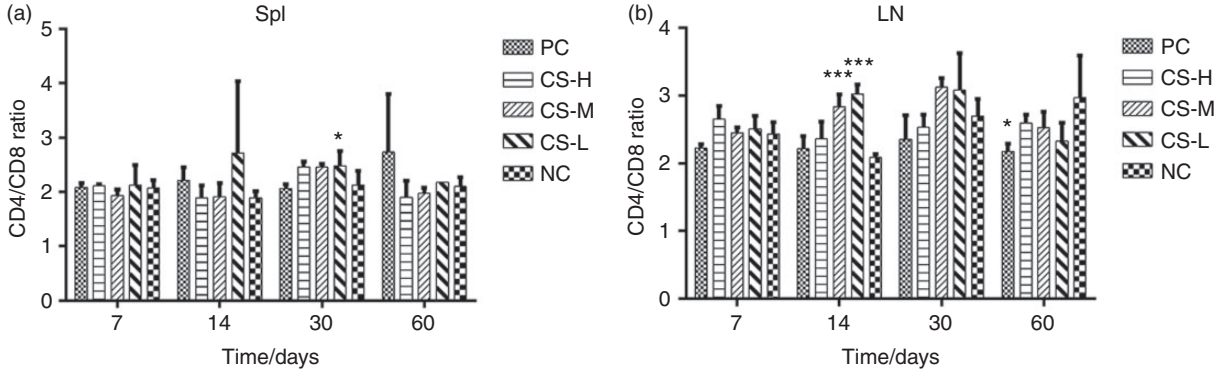

Figure 3. CD4+/CD8 + cell ratio calculated from flow cytometric plots of spleen (a) and lymph nodes (b) cells at varied time points. Spl: spleen; LN: lymph nodes.

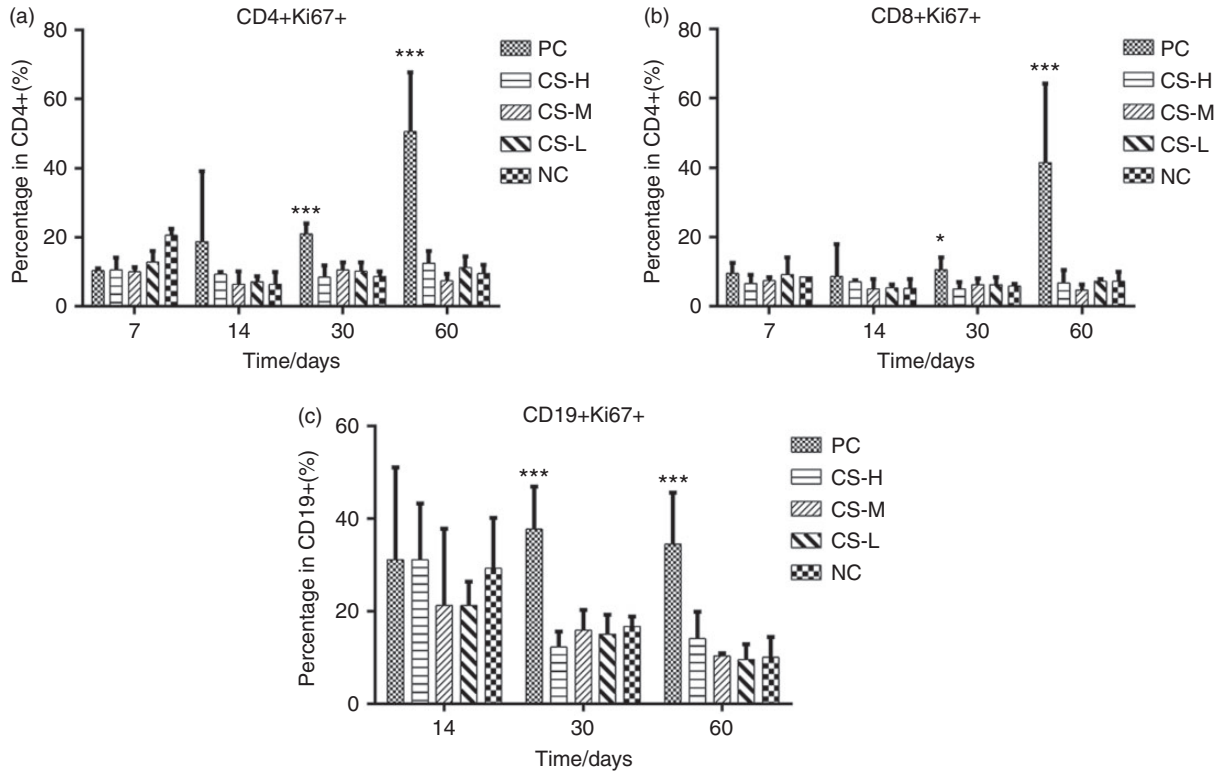

Figure 4. Ki67 + proportion in CD4 + T lymphocytes (a), CD8 + T lymphocytes (b), and CD19 + lymphocytes (c) in spleen at varied time points.

caused benign B lymphocytes proliferation in the early days.

Total IgG and IgM level in serum

IgM and IgG are two significant antibodies in humoral response, produced by B lymphocytes in primary and secondary immune response. The current study detected IgG and IgM secretion in serum by ELISA to determine humoral response level. IgM concentration was detected merely before day 14, as it is the first produced antibody in immune response and subsides quickly. It is clear in Figure 5(a) that IgM concentration of PC group reaches a peak by day 3, approximately 1000 μg/mL, then drops sharply by day 7, and keeps a comparatively normal level by day 14. IgM secretion in CS groups does not show apparent increase at any time points, almost retaining about 250 μg/mL and close to that in NC group. IgG secretion is following IgM but distinctly more abundant than it. Figure 5(b) illustrates that IgG secretion responds to the implants. Noticeably, CS groups do not produce abundant IgG to resist CS as PC group, but secret IgG concentration close to that in NC group, below 10 mg/mL. As for the difference among three experimental groups, it is statistically indistinguishable. These results are in accordance with those of IgM. Given this phenomenon, we consider CS implantation has not stimulated mice to secret elevated immunoglobulins, which demonstrates exceedingly weak humoral immune response. Moreover, the varied doses of CS do not exert a significant disparity with no implant in IgG and IgM secretion.

Cell infiltration around implants

To investigate local immune response brought by CS implantation, cell infiltration around implants was examined by H&E staining and the results are shown in Figure 6. At 7 and 14 days after immunization, mice implanted with BT and CS materials show remarkable cell infiltration surrounding implants. Differently, inflammatory cells infiltrate throughout BT but only on the edge of collagen. In addition, cell infiltration around CS is not as heavy as seen around BT. At day 30, a great piece of material retains in CS-H group but inflammatory cells population has decreased; in CS-M group, collagen fragments are still surrounded by inflammatory cells; in CS-L group, the material is absent and cell infiltration is unnoticeable. However, inflammation around BT is even more heavy and characterized by numerous inflammatory cells in PC group. At day 60, massive cells still infiltrate throughout BT in PC group, but no CS as well as inflammatory cells are

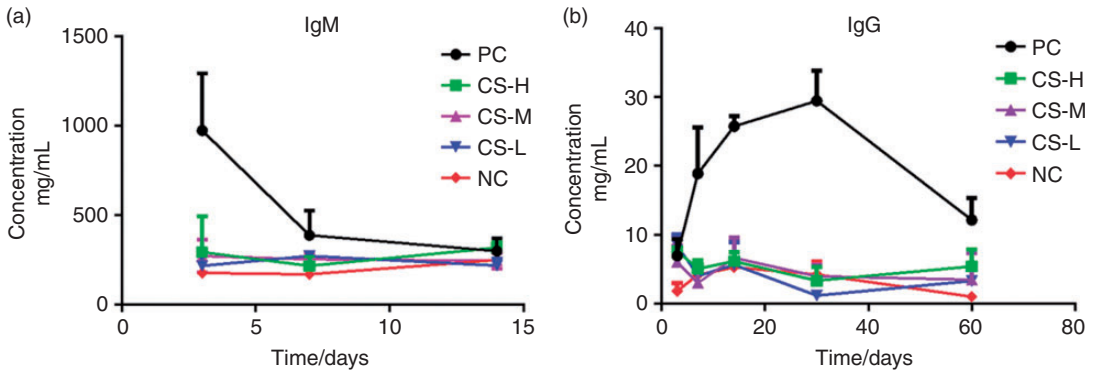

Figure 5. Concentration of IgM (a) and IgG (b) in serum at varied time points, detected by ELISA.

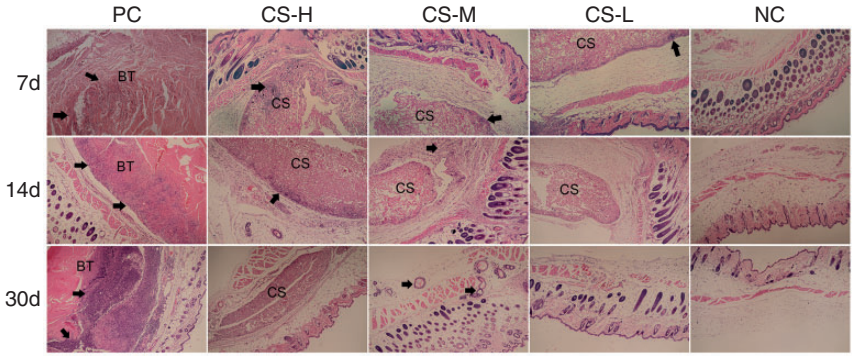

Figure 6. Representative images of H&E staining at implantation sites. Cell nuclei is stained blue. Cytoplasm, collagen fibres, elastic fibres and erythrocytes are stained different degrees of red. Obvious cell infiltration sites are marked with arrows, and implant materials are marked with BT and CS. Magnification is 100×.

present in all CS groups (data not shown). These results reveal that mice have slightly responded to CS by benign acute inflammation, as this kind of inflammation subsides with the progressive degradation of CS. Furthermore, higher dose of CS might have caused more violent and durable immune response.

TNF-α expression

TNF-α is an immunoregulatory cytokine, mainly secreted by macrophages, and it is closely relevant to inflammation. Therefore, TNF-α is used to determine the intensity of inflammation after implantation. In PC group, severe inflammation has occurred at 7, 14 and 30 days, because of consistently intense TNF-α immunostaining around BT (Figure 7), which indicates the implant has put consecutive stimulation on mice. However, in CS groups, TNF-α immunostaining is quite mild, far less than that in PC group. At day 7, evident immunostaining is observed in CS-M and CS-L, while scarcely positive immunostaining is observed in CS-H, indicating dinky difference among CS groups. At day 14 and 30, TNF-α expression in all CS groups has decreased gradually to the level of NC group. These images indicate that CS merely has triggered slight but obvious inflammation in the early days after implantation.

IFN-γ expression

IFN-γ is also a potent immunoregulatory cytokine, mainly produced by activated T lymphocytes and natural killer (NK) cells to boost Th1 cell proliferation, enhance the phagocytosis of macrophages and release of inflammatory mediators. As shown in Figure 8, IFN-γ staining is just distributed in scattered small dots at implantation sites. A little more IFN-γ is secreted around BT, especially in the slide of 14 days, compared to other groups. IFN-γ staining differences among the other groups are difficult to discover, even in the early period after implantation. By day 60, no noticeable CS is found in the slides, so images are not displayed. These results inform us that CS implantation has not engendered as strong inflammation as BT implantation.

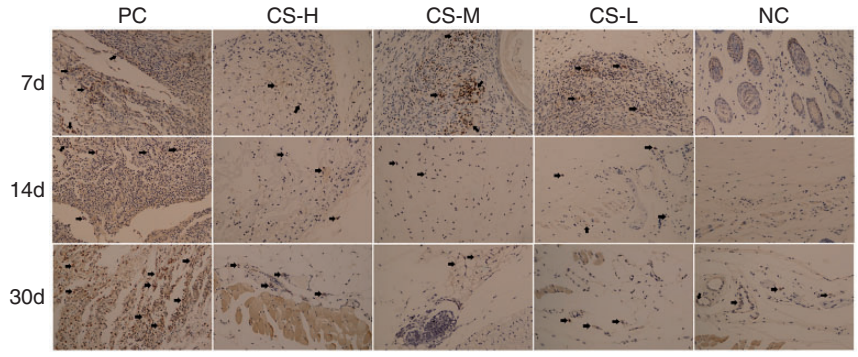

Figure 7. Representative images of TNF-α immunostaining around implants at day 7, 14, 30 post-implantations. In these images, obvious TNF-α staining is marked with arrows. All images were captured on an optical microscope at 200 × magnification.

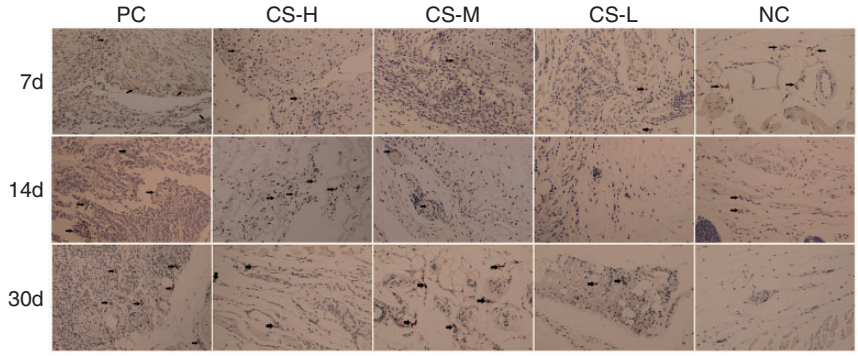

Figure 8. Representative images of IFN-γ expression around implants at day 7, 14, 30 post-implantations. In these images, obvious IFN-γ staining is signed with arrows. All images were captured on an optical microscope at 200 × magnification.

Discussion

Varied collagen forms, such as sponge,[1] membrane, plug,[14] gel, and multiple-original collagens, such as bovine, rat, fish,[34,35] plant,[9] have been applied to biomedical engineering. In previous study, when a new collagen form and varied source collagen was discovered, preliminary biocompatibility and immunogenicity evaluation were always performed. Nevertheless, some adverse reactions still occurred in clinic, like collagen allergy[36] and a granulomatous foreign-body reaction.[37]

In the current research, immune response evaluation of a new bovine sourced CS, acting as hemostats, was comprehensively evaluated in a mouse model, hoping to lay foundations for further studies on other animals and clinical trials. The present study was performed following three immunizations to acquire the maximum potential immune response, if existed. So immune response pattern should be adaptive immunity, and innate immunity (starts in a few hours) is not accessed. CS is used for hemostasis in a short time; however, it will stay in body for a long time until it degrades completely, as it also plays a significant role in promoting wound healing in middle and late period. Because we have proved that our CS degrades absolutely in 60 days in BALB/c mice, in order to better investigate acute and chronic immune response provoked by CS, we set the four time points.

Peripheral lymphoid organs were chosen to access immune response in previous studies. These organs are the main habitats of lymphocytes as well as immune response, so their sizes and weights can reflect immune response intensity in a way. Here, spleen and lymph nodes at varied time points after implantation are also accessed, but it is rough. Immune cells are examined from cell population, phenotype, proliferation ability and apoptosis to evaluate the immunogenicity of CS. Cell population in spleen and lymph nodes is coincident with morphology. Accordingly, we suppose that the increase of cell population partly contributes to the swelling of peripheral immune organs. Splenic cells proliferation in vitro under the stimulation of PMA and Iono was also assessed, because the proliferation ability can represent the transformation proportion of lymphoblasts, and the higher transformation proportion is, the more violent immune response is. Proliferating cells proportion is also detected by Ki67 immunostaining, since it can easily and accurately inform the type and population of proliferating cells.

As previously described, Ki67 is vital for cell proliferation, as it can bind to RNA and DNA by interacting with other proteins.[38] All these results demonstrate that immune stimulation brought by CS is relatively benign, moreover, apparent cell proliferation just occurred in CS-H group in the early days. In the current study, splenic cell apoptosis is defined as activation-induced cell death, as another indication of cell activation, thus, cell apoptosis should be accordant with cell proliferation theoretically. However, this measurement is conducted in vitro, and many factors, such as stimulant's dose and stimulating time, will complicate outcomes. Therefore, ideal cell apoptosis outcome in PC group is not obtained after seven days post-surgeries. Splenic cell population, lymphocytes proliferation and apoptosis in vitro become the potent evidences of dose effect; concretely, higher dose of CS initiates more noticeable immune response. CD4 + T lymphocytes, also called T helper lymphocytes, can assist B lymphocytes to secret antibody and promote T lymphocytes differentiation and maturation by secreting varied cytokines. CD8 + T lymphocytes, also called cytotoxic T lymphocytes, can directly kill tumors, infected cells and foreign cells without the assistance of antibody. The two cell types play a critical role in immune regulation. In normal state, the ratio of CD4+/CD8 + T lymphocytes is stable, even though their absolute number may be varied. From CD4/CD8 ratio of spleen in this study, we can speculate that immune function is in normal. CD4/CD8 ratio in lymph nodes is seemly complicated, but these differences cannot be regarded as consequences of immune rejection or destroyed immune function, because PC is not significantly different from NC at most time points, irrespective of CS groups, so we speculate individual difference among mice and experimental errors might contribute to these differences. In addition, ratios in CS and NC groups have small gaps, varying from 2.5 to 3, unlike PC group, in which ratio always lower than 2.5, so it can be inferred that CS do not lead to immune function disorder.

Many clinical researches discovered the elevated antibody level in patients received bovine collagen implant treatments but without adverse reaction.[39–41] However, antibody analysis by ELISA in our study demonstrates no obvious difference between mice with collagen implant and no implant. We suppose that this divergence with the previous clinical studies can be interpreted by the species variation, since another study was in agreement with our results and also illustrated no antibody resisting to bovine collagen was found in a rat model.[42] Actually, CD19+Ki67 + cell percentages at day 14 in CS and NC groups are slightly higher than those at day 30 and 60 in the present study (Figure 4(c)), and this finding is coincident with IgG concentration (Figure 5(b)). IgG concentration in CS and NC groups has increased from day 7 to 14 and decreased afterwards. These findings reveal minor humoral immune response has occurred in CS as well as NC groups.

As reported in other researches,[43,44] histological evaluation of tissue response to collagen shows marked cell infiltration around the implants, but this behavior resolves with the degradation of collagen. Chien et al.[44] found cell infiltration at collagen implantation sites was just on the outer rim of collagen scaffold in the early period. Similar tissue cellular reaction has been discovered in our study, but the difference is the cell type of infiltration. It should be noted that in early period of inflammation, neutrophils play a crucial role, while in middle and later period, infiltrating cells are primarily lymphocytes and monocytes. Once the body is sensitized by foreign antigen, another same stimulation may lead to the enhanced sensitization reaction, and this phenomenon is called hypersensitivity. Hypersensitivity caused by implants is called delayed type hypersensitivity, which is mediated mainly by T cell and characterized by mononuclear cell infiltration and tissue injury. Therefore, neutrophils infiltration was observed at days 1, 7, 14 post-implantation in the study of Chien et al., while infiltrating cell types are primarily T lymphocytes and macrophages in this study. These results inform us collagen implants can engender benign local tissue cellular reaction, but this response would not be everlasting.

TNF-α is one of the most important pro-inflammation cytokines, and it can promote cell adhesion to endodermis and migration to local inflammation sites by stimulating expression of selectins and chemotactic factors.[45] In the present study, TNF-α expression at implantation sites was examined by immunostaining. Remarkable positive TNF-α staining is observed in CS slides at day 7 and PC slides at all-time points, which demonstrate that benign and temporary inflammation has occurred in mice with CS implants, whereas heavy and persistent inflammation in mice with BT implants. TNF-α immunostaining informs us CS has evoked benign cellular response.

IFN-γ also plays a major role in inflammatory response, and its functions primarily consist of enhancing TNF-α production and activation, as well as the synergistic effect with TNF-α in inflammation. IFN-γ was proved to be a key cytokine of promoting inflammation in fat tissue in previous study.[46] However, in another study, IFN-γ was believed to function in a dual way in a Th1-dependant response. Concretely, it promoted inflammation in the early phase, whereas it acted as an inhibition cytokine to immune response in the late phase.[47] Here, no obvious IFN-γ immunostaining is examined in slides with CS, even in slides with PC, the positive IFN-γ immunostaining is moderate. Consequently, we suspect that immune stimulation

brought by CS implants and infection is benign, so no abundant IFN-γ is secreted to activate macrophages and induces major histocompatibility complex expression to enhance immune response.

Actually, even before these trials, we can make a general conclusion that the immune response is not so violent, for increasing trend in weight curves during the whole experimental period (shown in Supporting Information Figure S3). Expectantly, we find that even though noticeable immune response has arisen after CS implantation, the degree of response has declined with the degradation of collagen. Difference exerted by varied doses has not been discovered in most tests, it can be explained that the immunogenicity of CS is too low to distinguish the three doses. From the significant differences between BT and CS, we can also conclude that the CS is considerably pure and low immunogenic. Nevertheless, it should be aware that despite mild immune response triggered by CS has been evidenced in our study, further studies in different models remain to be performed to confirm the effectiveness and safety of this material.

As no comprehensive immunogenicity scheme has been reported in previous literatures, this study proposes a comparatively integrated and comprehensive scheme, covering macroscopic and microscopic indexes, cellular and humoral immune response, systematic and local analysis. Thus, this scheme is reasonable and can provide a reference for future immunogenicity evaluation of implantable biomaterials.

Conclusion

The major objective of this study is to build an immunogenicity evaluation scheme as well as detect immune response initiated by bovine sourced hemostatic CS in a mouse model. Marginal immune response is normally evoked by CS but a certain extent of immunologic reaction may be triggered at high dose. This kind of CS can be recognized as a qualified and promising hemostatic product for further researches. Meanwhile, the present scheme is appropriate for immunogenicity evaluation of all implantable biomaterials.

Authors' Note

Xufeng Niu and Wei Wang are both the corresponding authors of this article. Contact details of Xufeng Niu are: School of Biological Science and Medical Engineering, Beihang University, Beijing 100083, P. R. China. Email: nxf@buaa.edu.cn.

Acknowledgements

This study was performed with the assistance of Peking University Health Science Center for providing infrastructural facility and Guge Biological Technology Co., Ltd for technical supports. The authors appreciate the two units for their assistance.

Declaration of Conflicting Interests

The author(s) declared no potential conflicts of interest with respect to the research, authorship, and/or publication of this article.

Funding

The author(s) disclosed receipt of the following financial support for the research, authorship, and/or publication of this article: This work was supported by the National Natural Science Foundation of China (Nos. 31470915), the Fundamental Research Funds for the Central Universities (No. YWF-17-BJ-Y-45), the 111 Project (No. B13003), and the International Joint Research Center of Aerospace Biotechnology and Medical Engineering, Ministry of Science and Technology of China.

References

1. Geiger M, Li RH and Friess W. Collagen sponges for bone regeneration with rhBMP-2. *Adv Drug Delivery Rev* 2003; 55: 1613–1629.
2. Ferreira AM, Gentile P, Chiono V, et al. Collagen for bone tissue regeneration. *Acta Biomater* 2012; 8: 3191–3200.
3. Pek YS, Gao S, Arshad MS, et al. Porous collagen-apatite nanocomposite foams as bone regeneration scaffolds. *Biomaterials* 2008; 29: 4300–4305.
4. Inzana JA, Olvera D, Fuller SM, et al. 3D printing of composite calcium phosphate and collagen scaffolds for bone regeneration. *Biomaterials* 2014; 35: 4026–4034.
5. Zugravu MV, Smith RA, Reves BT, et al. Physical properties and in vitro evaluation of collagen-chitosan-calcium phosphate microparticle-based scaffolds for bone tissue regeneration. *J Biomater Appl* 2013; 28: 566–579.
6. Liu Z, Yin X, Ye Q, et al. Periodontal regeneration with stem cells-seeded collagen-hydroxyapatite scaffold. *J Biomater Appl* 2016; 31: 121–131.
7. Liu J, Argenta L, Morykwas M, et al. Properties of single electrospun poly (diol citrate)-collagen-proteoglycan nanofibers for arterial repair and in applications requiring viscoelasticity. *J Biomater Appl* 2014; 28: 729.
8. Judd O, Mcclelland L and Sharp JF. Porcine dermal collagen graft for tracheoesophageal fistula repair. *Otolaryngol Head Neck Surg* 2010; 142: 444–445.
9. Willard JJ, Drexler JW, Das A, et al. Plant-derived human collagen scaffolds for skin tissue engineering. *Tissue Eng Part A* 2013; 19: 1507–1518.
10. Boyce ST, Christianson DJ and Hansbrough JF. Structure of a collagen-GAG dermal skin substitute optimized for cultured human epidermal keratinocytes. *J Biomed Mater Res Part A* 1988; 22: 939–957.
11. Helary C, Bataille I, Abed A, et al. Concentrated collagen hydrogels as dermal substitutes. *Biomaterials* 2010; 31: 481–490.
12. Gaspar A, Moldovan L, Constantin D, et al. Collagen-based scaffolds for skin tissue engineering. *J Med Life* 2011; 4: 172–177.

13. Niu X, Feng Q, Wang M, et al. Porous nano-HA/collagen/PLLA scaffold containing chitosan microspheres for controlled delivery of synthetic peptide derived from BMP-2. *J Controll Release* 2009; 134: 111–117.
14. Kallmes DF, Mcgraw JK, Li ST, et al. In vivo evaluation of a new type I collagen hemostatic plug for high-risk, large-core biopsies. *J Vasc Interv Radiol* 1998; 9: 656–659.
15. Hait MR, Robb CA, Baxter CR, et al. Comparative evaluation of Avitene microcrystalline collagen hemostat in experimental animal wounds. *Am J Surg* 1973; 125: 284–287.
16. Jiang X, Wang Y, Fan D, et al. A novel human-like collagen hemostatic sponge with uniform morphology, good biodegradability and biocompatibility. *J Biomater Appl* 2017; 31: 1099–1107.
17. Farndale RW, Sixma JJ, Barnes MJ, et al. The role of collagen in thrombosis and hemostasis. *J Thromb Haemostasis* 2004; 2: 561–573.
18. Sirlak M, Eryilmaz S, Yazicioglu L, et al. Comparative study of microfibrillar collagen hemostat (Colgel) and oxidized cellulose (Surgicel) in high transfusion-risk cardiac surgery. *J Thorac Cardiovasc Surg* 2003; 126: 666–670.
19. Beil W, Timpl R and Furthmayr H. Conformation dependence of antigenic determinants on the collagen molecule. *Immunology* 1973; 24: 13–24.
20. Allaire E, Guettier C, Bruneval P, et al. Cell-free arterial grafts: morphologic characteristics of aortic isografts, allografts, and xenografts in rats. *J Vasc Surg* 1994; 19: 446–456.
21. Delustro F, Condell RA, Nguyen MA, et al. A comparative study of the biologic and immunologic response to medical devices derived from dermal collagen. *J Biomed Mater Res Part A* 1986; 20: 109–120.
22. Dahm M, Lyman WD, Schwell AB, et al. Immunogenicity of glutaraldehyde-tanned bovine pericardium. *J Thorac Cardiovasc Surg* 1990; 99: 1082–1090.
23. Tsuda H, Higashi S, Iwanaga S, et al. Development of antitissue factor antibodies in patients after liver surgery. *Blood* 1993; 82: 96–102.
24. Peng YY, Glattauer V, Ramshaw JA, et al. Evaluation of the immunogenicity and cell compatibility of avian collagen for biomedical applications. *J Biomed Mater Res Part A* 2010; 93: 1235–1244.
25. Dilgimen AS, Mustafaeva Z, Demchenko M, et al. Water-soluble covalent conjugates of bovine serum albumin with anionic poly(N-isopropyl-acrylamide) and their immunogenicity. *Biomaterials* 2001; 22: 2383–2392.
26. Ziv O, Avtalion RR and Margel S. Immunogenicity of bioactive magnetic nanoparticles: natural and acquired antibodies. *J Biomed Mater Res Part A* 2008; 85: 1011–1021.
27. Kreiser S, Eckhardt J, Kuhnt C, et al. Murine CD83-positive T cells mediate suppressor functions in vitro and in vivo. *Immunobiology* 2015; 220: 270–279.
28. O'Donnell H, Pham OH, Li LX, et al. Toll-like receptor and inflammasome signals converge to amplify the innate bactericidal capacity of T helper 1 cells. *Immunity* 2014; 40: 213–224.
29. Bao LQ, Dang MN, Huy NT, et al. Splenic CD11c(+) cells derived from semi-immune mice protect naïve mice against experimental cerebral malaria. *Malar J* 2015; 14: 23–23.
30. Liu H, Wise SG, Rnjak-Kovacina J, et al. Biocompatibility of silk-tropoelastin protein polymers. *Biomaterials* 2014; 35: 5138–5147.
31. Pandit AS, Feldman DS and Caulfield J. In vivo wound healing response to a modified degradable fibrin scaffold. *J Biomater Appl* 1998; 12: 222–236.
32. Rosenberg GA, Cunningham LA, Wallace J, et al. Immunohistochemistry of matrix metalloproteinases in reperfusion injury to rat brain: activation of MMP-9 linked to stromelysin-1 and microglia in cell cultures. *Brain Res* 2001; 893: 104–112.
33. Tseng H, Balaoing LR, Grigoryan B, et al. A three-dimensional co-culture model of the aortic valve using magnetic levitation. *Acta Biomater* 2014; 10: 173–182.
34. Song E, Yeon KS, Chun T, et al. Collagen scaffolds derived from a marine source and their biocompatibility. *Biomaterials* 2006; 27: 2951–2961.
35. Pati F, Datta P, Adhikari B, et al. Collagen scaffolds derived from fresh water fish origin and their biocompatibility. *J Biomed Mater Res Part A* 2012; 100: 1068–1079.
36. Nelson PA, Powers JN, Estridge TD, et al. Serological analysis of patients treated with a new surgical hemostat containing bovine proteins and autologous plasma. *J Biomed Mater Res Part A* 2001; 58: 710–719.
37. Mcgregor DH, Macarthur RI and Carter T. Avitene granulomas of colonic serosa. *Ann Clin Lab Sci* 1986; 16: 296–302.
38. Maccallum DE and Hall PA. The location of pKi67 in the outer dense fibrillary compartment of the nucleolus points to a role in ribosome biogenesis during the cell division cycle. *J Pathol* 2000; 190: 537–544.
39. Jr MCJ, Schade WJ, Siegle RJ, et al. Characterization of the humoral immune response to bovine collagen implants. *Arch Dermatol* 1985; 121: 990–994.
40. Cooperman L and Michaeli D. Immunogenicity of injectable collagen. II. A retrospective review of 72 tested and treated patients. *J Am Acad Dermatol* 1984; 10: 647–651.
41. Jr MCJ, Schade W, Siegle RJ, et al. Immune responses to bovine collagen implants: significance of pretreatment serology. *J Am Acad Dermatol* 1987; 16: 955–960.
42. Anselme K, Bacques C, Charriere G, et al. Tissue reaction to subcutaneous implantation of a collagen sponge. A histological, ultrastructural, and immunological study. *J Biomed Mater Res Part A* 1990; 24: 689–703.
43. Unsal B, Kurtiş B, Ozcan G, et al. An investigation of resorption and tissue reaction after subcutaneous implantation of collagen based membrane materials in rats. *J Marmara Univ Dent Fac* 1997; 2: 609–615.
44. Chien KB, Aguado BA, Bryce PJ, et al. In vivo acute and humoral response to three-dimensional porous soy protein scaffolds. *Acta Biomater* 2013; 9: 8983–8990.
45. Zelová H and Hošek J. TNF-α signalling and inflammation: interactions between old acquaintances. *Inflammation Res* 2013; 62: 641–651.
46. Rocha VZ, Folco EJ, Sukhova G, et al. Interferon-gamma, a Th1 cytokine, regulates fat inflammation a role for adaptive immunity in obesity. *Circ Res* 2008; 103: 467–476.
47. Feuerer M, Eulenburg K, Loddenkemper C, et al. Self-limitation of Th1-mediated inflammation by IFN-gamma. *J Immunol* 2006; 176: 2857–2863.

http://bhxb.buaa.edu.cn jbuaa@buaa.edu.cn
DOI: 10.13700/j.bh.1001-5965.2017.0230

可吸收胶原膜的体内免疫反应评价

张林, 孙磊, 徐梦洽, 牛旭锋*

(北京航空航天大学 生物与医学工程学院, 北京 100083)

摘 要: 免疫应答反应一直是限制可植入生物材料应用的关键因素之一。本实验评估了2种用于骨修复的胶原膜在体内的免疫反应,希望为其临床试验提供依据。在将2种膜皮下植入到BALB/c小鼠后的第14天,与阴性对照(NC,未植入材料)相比,脾和淋巴结没有明显肿大,淋巴结细胞数几乎没差异,而脾细胞数大约是NC的2倍。流式细胞术分析显示植入胶原膜1导致脾中T细胞比例减少了约13%,但是没有影响T细胞亚群,而植入胶原膜2对小鼠的脾细胞组成没有明显影响;2种胶原膜都激活了一定的B细胞,激活率大约为NC小鼠的2倍。淋巴细胞体外增殖实验显示与NC组无显著差异。酶联免疫吸附测试表明胶原膜1导致了第14天血清中的抗体浓度升高至NC小鼠的2倍。局部H&E染色显示2种材料都引起了轻微的细胞浸润。这2种胶原膜引起的免疫反应很微弱,可以被应用于临床试验。

关 键 词: 胶原膜; 骨修复; 免疫应答; 流式细胞术; 炎症

中图分类号: R318.06

文献标识码: A **文章编号**: 1001-5965(2018)04-0879-08

引导组织再生术(Guided Tissue Regeneration, GTR)常用于牙周修复,主要是在伤口处使用一种闭塞膜形成一种物理屏障,阻止牙结缔组织向牙根面生长,为牙周膜、牙骨质和牙槽骨的修复提供空间和时间。GTR已经被提出作为根管治疗的辅助手段来促进骨再生[1],并且使用GTR以促进牙周再生已经取得了满意的结果[2],尤其在较严重的根尖周病变和贯穿病变的情况下。目前的研究发现,使用可吸收的屏障材料比不可吸收的材料,或者不使用屏障材料的效果要好[1]。理想的屏障材料需满足以下几个条件:生物相容的,能够作为屏障防止其他细胞类型向根面生长,允许营养物质和空气通过,允许组织整合进材料却又不影响其防止内皮细胞向下生长的功能,提供并维持一个靠近根面的空间,具有便于加工的结构等[1]。

胶原已经被用于骨修复,不仅因为它是骨基质的主要成分,具有良好的生物相容性和生物降解性,无细胞毒性,较低的免疫原性,易被加工成为不同的形式[3]。此外,胶原还是一种牙周膜成纤维细胞的趋化因子[4],能够阻挡内皮细胞的迁移,并且具有止血效应[5]。在胶原作为屏障材料的研究中都发现了牙再生的现象,并且5个月之后胶原全部降解[6]。可见,胶原作为引导膜治疗牙周病具有一定的优势,是一种较理想的材料,所以用于牙修复的胶原膜被广泛研究,但是其能否成为广泛应用的产品还得经过另一项检测,也就是免疫学评价,因为免疫原性是产生免疫毒性的主要原因。

众所周知,大多数胶原都来源于动物,因而提取的胶原中残留动物蛋白、DNA、细胞是难以避免的。有研究表明,胶原的结构、其中残留的非胶原

收稿日期: 2017-04-13; **录用日期**: 2017-05-19; **网络出版时间**: 2017-06-16 16:10
网络出版地址: kns.cnki.net/kcms/detail/11.2625.V.20170616.1610.002.html
基金项目: 国家自然科学基金(31470915); 中央高校基本科研业务费专项资金(YWF-17-BJ-Y-45)
* **通信作者**. E-mail: nxf@buaa.edu.cn

引用格式: 张林, 孙磊, 徐梦洽, 等. 可吸收胶原膜的体内免疫反应评价[J]. 北京航空航天大学学报, 2018, 44(4): 879-886.
ZHANG L, SUN L, XU M H, et al. Immunological response evaluation of absorbable collagen membrane in vivo[J]. Journal of Beijing University of Aeronautics and Astronautics, 2018, 44(4): 87[illegible]6 (in Chinese).

蛋白和细胞、胶原的交联方式等都会对胶原的免疫原性产生影响[7]。因此,为了病人的安全和产品的广泛使用,进行免疫原性评价是十分必要的。

以往也有类似的研究,但是他们的研究都不够深入全面,大多都只是停留在炎症的研究,而组织学检验和抗体检测是使用最广泛的评价方法[8-10]。在本实验中对猪来源的 2 种骨导膜进行了免疫学评价,希望为其广泛的应用于临床奠定基础。本实验制定了一套较完整的免疫原性检测方案,通过将其植入到 BALB/c 小鼠皮下,定期取样检测来分析胶原膜引起的免疫应答反应,检测指标涵盖了细胞免疫和体液免疫,局部免疫和系统免疫,免疫器官、免疫细胞和免疫分子,对胶原膜的临床应用具有重要意义。

1 实 验

1.1 动物与材料

动物实验已经获得了北京大学医学部动物伦理委员会的批准,并严格按照其规定来饲养动物。本实验共需要 20 只 6 ~ 8 周,体重 20 g 左右的雌性 BALB/c 小鼠,实验共分为 4 组,每组 5 只,包括 2 个试验组(S1 和 S2,分别植入胶原膜 1 和胶原膜 2),阳性对照组(PC,植入猪皮),阴性对照组(NC,只做手术,不植入)。材料由深圳兰度生物材料有限公司提供。

1.2 皮下植入

以 50 mg/kg 的比例腹腔注射 w/v 分数 0.5% 的戊巴比妥钠生理盐水溶液麻醉小鼠,待小鼠昏迷之后,选取一块背部脊柱两侧的皮肤,脱毛并用体积分数 75% 酒精消毒,用无菌手术剪剪开一个约 1 cm 的伤口并撑开皮肤,放入材料,缝合伤口(NC 组不植入直接缝合)。总共在每只老鼠背部 3 个不同位置皮下植入各 1 次,一周一次。

1.3 取 样

1.3.1 取 血

分别在 3 次植入后第 3 天和第 7 天,分别剪去约 1 cm 长度的尾尖取血,用 EP 管收集,待血液分层之后,10 000 r/min 离心 5 min,收集上清液于另一干净的 EP 管,标记,置于 -20 ℃ 冰箱供检测抗体。到第 14 天时,直接摘除一只眼球取血,后面的处理同上。

1.3.2 脏器处理

第 14 天取血之后,拉颈处死小鼠,无菌环境下摘除脾和腋下淋巴结,浸泡于无菌磷酸盐缓冲液(Phosphate Buffer Solution, PBS)中。将脾脏研磨成单细胞悬液,800 r/min 离心 5 min,去上清,加入 1 mL 红细胞裂解液,室温 1 min,再加 PBS 至 5 mL以终止反应,离心去上清,加入一定量 PBS 悬浮细胞并混匀。取出少量稀释到适当倍数,进行细胞计数。淋巴结也经过类似的处理,只是不需要加红细胞裂解液,直接稀释计数。

1.3.3 局部组织处理

剪下最后一次植入部位的皮肤和材料,浸泡于 4% 多聚甲醛中固定,供组织学分析。

1.4 细胞表型和流式细胞术

用于脾细胞表型识别和筛选的 5 种荧光单克隆抗体分别是 anti-CD19 PE-Cy7、anti-TCR APC、anti-CD4 FITC、anti-CD8 PerCP、anti-Ki67 PE。将单细胞悬液加入 2 mL 圆底离心管中,1 500 r/min 离心 5 min,弃上清液。加冷 PBS 1 mL,离心洗涤,弃上清液。加入用 PBS 稀释的荧光素标记的抗体 200 μL。用微量移液器轻轻吹打混匀,4 ℃ 或置冰上孵育 30 min ~ 1 h。离心弃上清液,加入冷 PBS 1 mL,离心洗涤 2 次,以除去未结合的多余抗体成分。向细胞中加入冷 PBS 500 μL,吹打混匀,置流式管中,4 ℃ 避光保存,待测[11-12]。

1.5 细胞增殖

按每孔 2×10^5 的细胞数量取得细胞,离心去上清,加入 1640 培养基(含体积分数 10% 胎牛血清,体积分数 1% 双抗)200 μL,并按比例加入佛波酯(Phorbol-12-Myristate-13-Acetate, PMA)和离子霉素(Ionomycin, Iono)使之终浓度为 100 ng/mL 和 1 000 ng/mL,混匀后加入 96 孔板,入二氧化碳培养箱培养。48 h 后用 MTS 试剂盒检测细胞增殖情况,具体来说,取出孔板,小心吸出上层培养液,每孔加 20 μL MTS 和 80 μL 1640 培养液混合液,培养箱孵育 1 h,用酶标仪测 490 nm 处的吸光度。

1.6 酶联免疫吸附测试

用包被液以 1∶1 000 稀释包被抗体,每个孔 100 μL,4 ℃ 过夜孵育。倒去包被液,每孔加入 200 μL PBST(体积分数 0.05% 吐温-20 的 PBS 溶液)洗涤 1 min,洗 3 次,用纱布包住拍干水分。加入 200 μL PBSB(w/v 分数 1% 牛血清白蛋白的 PBS 溶液)封闭液,室温放置 2 h 后,倾去液体,拍干水分。加入稀释好的样品(IgG 1∶100 000,IgM 1∶10 000)以及标准品(IgG1∶25000,IgM1∶5 000)100 μL,并设置空白对照,室温 2 h。洗涤 6 次,拍干水分。辣根过氧化物酶标记的一抗用 PBSB 稀释 1 000 倍,每孔加 100 μL,室温 2 h,洗涤 6 次,拍干。加 100 μL 3,3′,5,5′-四甲基联苯胺,

黑暗孵育 10 min(IgM)/20 min(IgG)后,加 50 μL 终止液(2 mol/L 硫酸溶液),450 nm 测吸光度[13]。

1.7　H&E

如文献[14]所述,皮肤组织经过 w/v 分数 4% 多聚甲醛固定之后,经过水洗,酒精梯度脱水,透明,石蜡包埋。石蜡块被切成 3 ~ 5 μm 的薄片,置于载玻片上,脱蜡之后再进行 H&E 染色,按标准步骤进行。

1.8　数据处理

所有数据都是由至少 3 个平行样本得出的,数据显示为 mean ± SD (均值 ± 标准差),作图是采用 GraphPad Prism 软件,数据分析采用的是单因素方差分析,当 $^{*}p<0.05$, $^{**}p<0.01$, $^{***}p<0.005$ 时,差异被视为具有统计学意义,文中所有比较都是与 NC 组比。

2　结果与讨论

2.1　免疫器官及细胞计数

脾和淋巴结是淋巴细胞的主要栖息地,也是免疫反应发生的主要场所,因此观察脾和淋巴结的大小以及其中的免疫细胞数目能从一定程度上反映免疫反应的强弱。图 1 所示为 3 次免疫后第 14 天时小鼠的脾和淋巴结的形态,可以看到 S1 和 S2 组的脾和淋巴结与正常的脾和淋巴结对比,都没有表现出明显的大小变化,而 PC 组的脾出现了剧烈的膨大,比 NC 组的 2 倍还大,淋巴结也明显较大。脾细胞计数结果见图 2(a),2 个试验组的脾细胞数约为 2×10^{8},稍高于 NC 组的 1×108,但差异无统计学意义。而 PC 组细胞数目也正如看到的急剧膨大的脾一样,远远高于 NC 组,约 4.7×10^{8}。淋巴结细胞数目见图 2(b),无论是 PC 组还是 2 个试验组,都与 NC 组的差异无统计意义,但是也能看到 PC 的淋巴结中的细胞数目(约8.5×10^{7})高于其他组,约是NC组(约2.8×10^{7})的 3 倍。无论是免疫器官还是其中的免疫细胞数目,结果都基本一致,即 2 种胶原膜对小鼠的免疫刺激都较小。

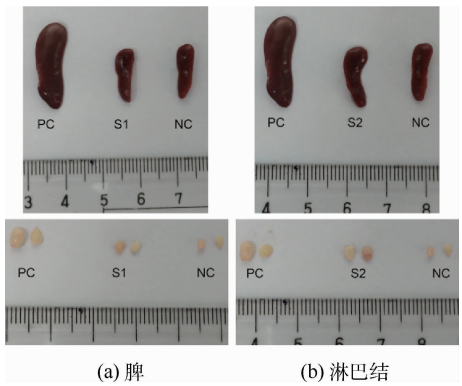

图 1　脾和淋巴结形态

Fig. 1　Images of spleen and lymph nodes

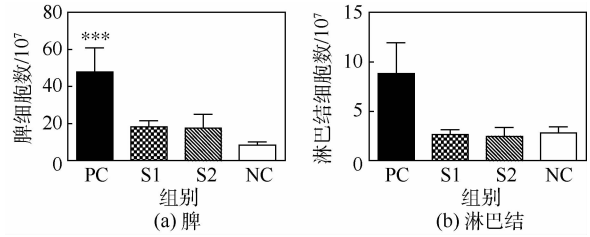

图 2　脾和淋巴结的免疫细胞计数结果($^{***}p<0.005$)

Fig. 2　Immune cell population of spleen and lymph nodes ($^{***}p<0.005$)

2.2　脾淋巴细胞表型

正常脾淋巴细胞中 T 细胞约占 40%,B 细胞占 60%,CD4/CD8 = 2∶1。CD4 + T 细胞与 CD8 + T 细胞的比值变化能从一定程度上反应机体的免疫功能状态。本实验分析了脾淋巴细胞的表型,每个组有 3 个平行样本,规律类似,代表性流式图如图 3 所示,图中比例表示对应类别细胞占总测试细胞的比例。由图 3 可得到各组脾细胞中 CD4 + T细胞、CD8 + T 细胞和 B 细胞的含量百分比。对比试验组和对照组结果可以得出,S2 组的脾细胞组成比例正常,与 NC 组无明显差异;S1 组中,脾内 T 细胞比例减少了约 13%,B 细胞比例轻微增多,但整体变化较 PC 组(T 细胞比例与正常组比较下降了约 22%,T、B 细胞比例明显失衡)明显更小。且对比正常 T 细胞亚群 CD4/CD8 比例(约 2.3)可知 S1 组和 S2 组 CD4/CD8 比例(分别为 2.1 和 2.5)正常;而 PC 组 CD4/CD8 比偏低(约 1.5)。由此实验结果可初步得出结论,胶原膜 1 的植入会引起小鼠轻微的免疫应答反应,但未影响其免疫系统的正常机能;而胶原膜 2 对小鼠的影响极小。

2.3　脾淋巴细胞活化

T 细胞的活化通过 2 个亚群 CD4 + 细胞和 CD8 + 细胞反映,B 细胞的活化则通过 CD19 + 细胞反映。本实验对 CD4 +,CD8 + 和 CD19 + 细胞表面的 Ki67 表达进行了检测,因为 Ki67 是与细胞活化和增殖相关的分子。每个组有 3 个平行样本,规律类似,代表性的流式分析图如图 4 所示。通过结果(图4)可以看出,各组别的CD4 + 和 CD8 + T 细胞的活化状态无太大区别,但还是能看出 PC 组和 S1 组的 CD4 + T 细胞活化相对较多,活化比例比 NC 组高出约 5%;S1 组和S2 组的B细胞活化稍有增加,约为NC组(5.14%)的

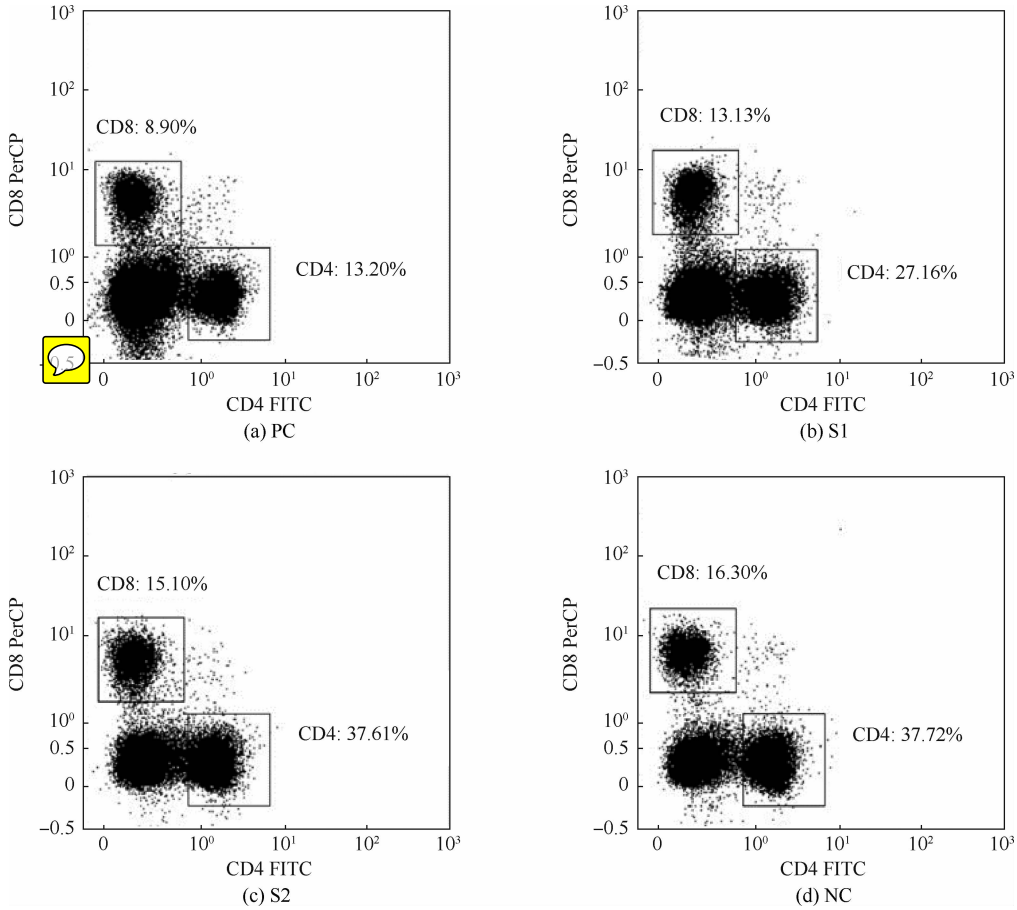

图 3 流式细胞术分析脾细胞表型

Fig. 3 Splenic cells' phenotype analysis by flow cytometry

2 倍,但 S1(13.29%)多于 S2(9.61%),PC 组 B 细胞明显处于过度活跃状态中,活化率高达 19.64%,大约是 NC 组的 4 倍。这些结果表明植入胶原膜引起了适当的免疫细胞激活,即小鼠对胶原膜作出了轻微免疫反应,对比 2 种胶原膜,胶原膜 1 引起的反应更明显。

2.4 淋巴细胞增殖

水溶性甲臜化合物(MTS)能被细胞线粒体中的脱氢酶还原为具有高度水溶性的有色甲臜产物,生成的甲臜物的数量与活细胞的数量成正比。用酶标仪在 490 nm 波长处测定其光吸收值,可间接反映活细胞数量。淋巴细胞的增殖能力代表了其向淋巴母细胞的转化情况,而淋巴母细胞的转化率可以反映免疫反应水平。本实验采用 PMA 和 Iono 体外刺激细胞增殖来检测细胞的活化情况,结果如图 5 所示,图中 ** 表示 PC 组和 NC 组的吸光度差异具有高度的统计学意义。植入胶原膜第 14 天之后的老鼠的脾细胞和淋巴结细胞,均没有像 PC 组细胞那样表现出显著高于正常小鼠细胞的增殖能力,吸光度都在 0.5 左右,与正常小鼠的差异无统计学意义,也就是说明材料没有刺激大量的免疫细胞活化,即免疫反应微弱。

2.5 血清中抗体水平

抗体是由浆细胞分泌的用来鉴别和中和外来抗原的物质,在体液免疫中起着重要的作用。本实验检测了血清中的 IgM 和 IgG,它们分别在初次免疫应答和再次免疫应答中起作用,因此 IgG 产生较晚。酶联免疫吸附测试结果显示各组中 IgM 浓度没有显著差异(图 6 中未显示)。对此分析这可能是因为在 3 次植入免疫中,第 1 次植入时机体免疫主要为初次免疫应答,IgM 水平较高;随着后续增强免疫的进行,机体免疫应答逐渐以再次应答为主,初次应答的水平逐渐减弱,故在 3 次免疫后第 3 天检测时机体初次应答水平已经处于较弱阶段,因此 IgM 浓度整体水平较低,故 4 组小鼠组间无明显差异。IgG 浓度的检测结果如图 6 所示,S1 组的 IgG 浓度一直处于上升趋势,但曲线斜率明显小于 PC 组,S1 组第 14 天血清中的 IgG 浓度(约 12 mg/mL)约是 NC 组(约 5.5 mg/mL)的 2 倍;而 S2 组的 IgG 浓度在第 7 天出现了轻微地上升,从 4 mg/mL 到 8 mg/mL,第 14 天时与第7天差别不大。总体来说,2个试验组

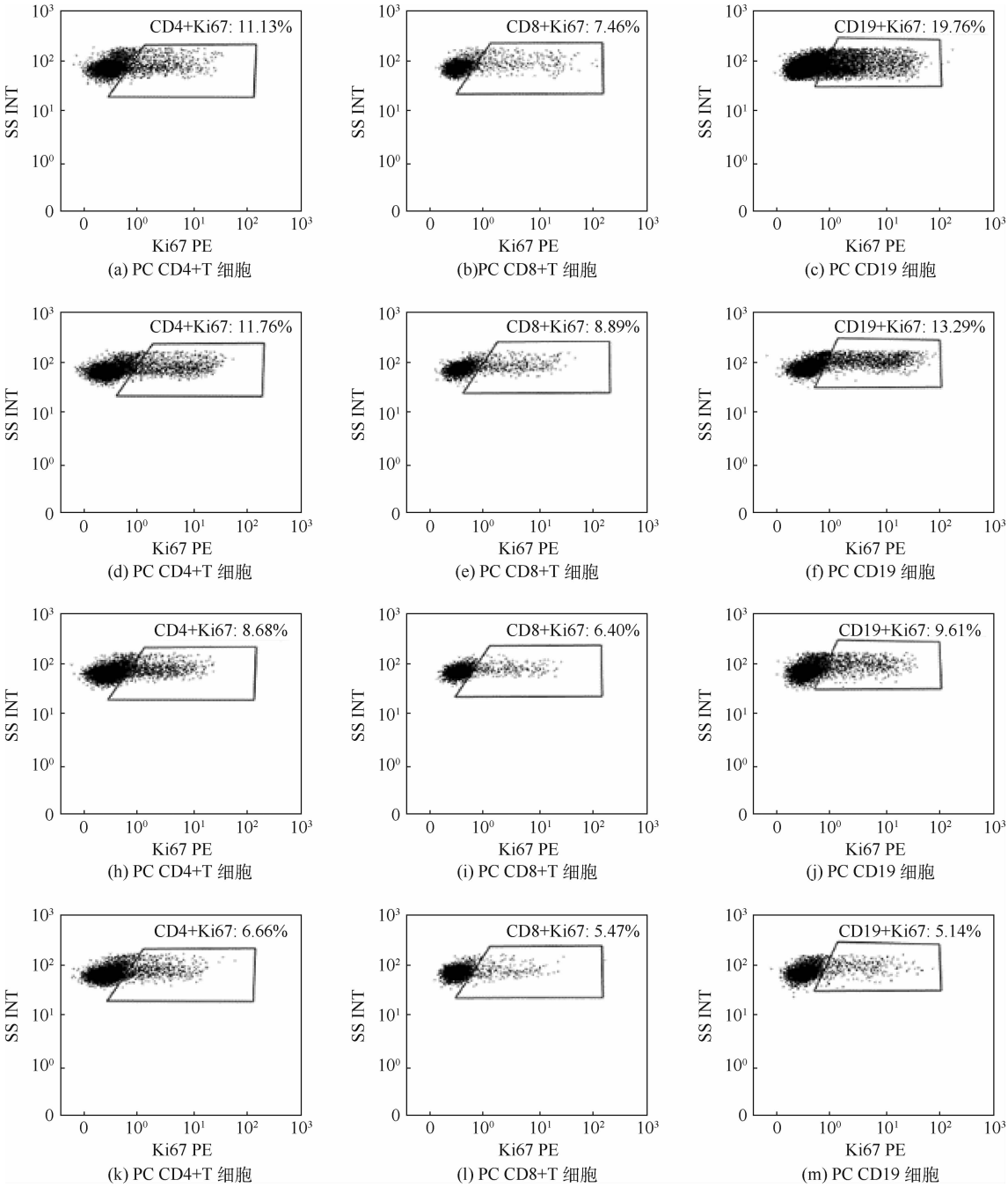

图 4　CD4 + T 细胞、CD8 + T 细胞和 CD19 + 细胞的 Ki67 表达情况

Fig. 4　Ki67 expression of CD4 + T lymphocytes, CD8 + T lymphocytes and CD19 + lymphocytes

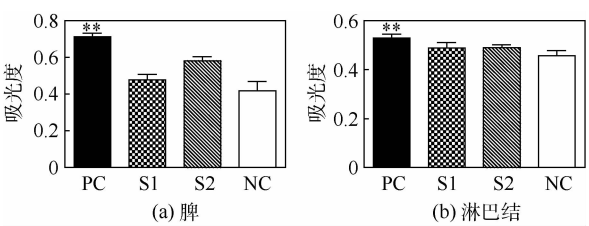

图 5　脾和淋巴结细胞体外增殖情况（$^{**}p<0.01$）

Fig. 5　Proliferation in vitro of splenic cells and lymph nodes cells ($^{**}p<0.01$)

与 NC 组的 IgG 浓度变化差异不大,尤其是S2 组。Liu 等[15]也有类似的发现,将猪源Ⅰ型胶原膜作为角膜原位移植到 BALB/c 小鼠后,在第 14 天的血清中也检测到了 IgG,并且浓度随时间升高。而 Patino 等[16]的研究表明在 Wistar 大鼠的血清中没有检测到针对猪源胶原膜的抗体,这种差异可能是由于动物的种类不同而导致的。由此可见,本实验中的猪来源的胶原膜 1 有可能对小鼠产生了一定的刺激作用,以至于小鼠体内产生了适当的 IgG 抗体来中和这种外来抗原,而胶原膜 2 对小鼠的刺激是不明显的。

2.6　细胞浸润

以上的实验都是针对系统性的免疫反应,这

项测试则是用来评价局部免疫反应。局部炎症反应的一个特征是炎性细胞浸润,因此在本实验中笔者采用 H&E 染色来检查植入局部的炎症发生情况。代表性的 H&E 染色如图 7 所示,M 为植入的材料,右图是左图的局部放大。植入之后第 14 天,在 PC 组的组织中,大量的细胞聚集在整个材料之中,也就是说炎症反应剧烈;与未植入的皮肤相比,在胶原膜 1 和胶原膜 2 的周围有稍多的细胞浸润,并且胶原膜 1 周围的细胞数量多于胶原膜2,但都只是围绕在材料周围。这种现象

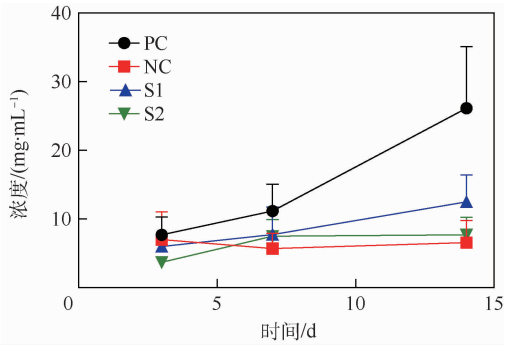

图 6 血清中 IgG 浓度随时间的变化

Fig. 6 Variation of concentration of IgG in serum with time

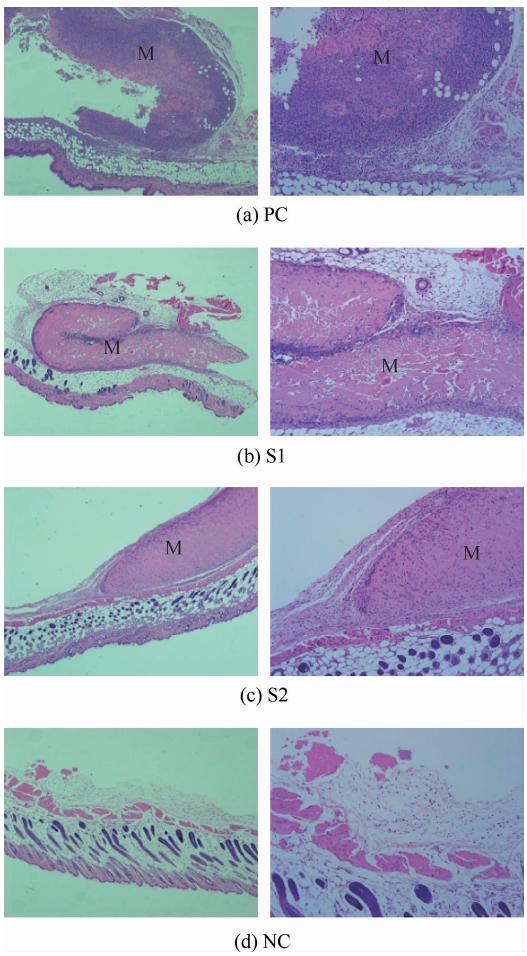

图 7 植入部位 H&E 染色

Fig. 7 H&E staining of implantation sites

与以往的研究结果一致,Liu 等[15]的研究在植入后第 12 天也发现细胞浸润现象只发生在胶原材料周围,而没有侵入其中。猜测可能是由于胶原本身的免疫原性比较低,以至于浸润细胞少且细胞浸润的速度慢。由此可见这 2 种材料会引起轻微的局部炎症反应,并且胶原膜 1 引起的炎症稍强于胶原膜 2。

本文实验中的 2 种胶原膜唯一的差别在于胶原膜 1 是经过了过氧化氢灭菌处理,而胶原膜 2 没有。过氧化氢是一种强氧化剂,它灭活微生物的原理是通过解离高活性的羟基,攻击破坏微生物的细胞壁、DNA、脂类以及蛋白质等,对包膜病毒作用尤为明显,生成产物只有水和氧气,广泛应用于生物医药领域[17-18]。本实验中几乎所有的结果都表明胶原膜 1 在 BALB/c 小鼠中引起的免疫反应明显强于胶原膜 2,推测主要原因是过氧化氢破坏了胶原的结构,使之抗原决定簇更多地暴露,从而增强了其免疫原性。有研究结果表明[19],当过氧化氢浓度低于 2%(体积分数)时,主要以氧化基团与胶原的交联为主,而当过氧化氢浓度达到 3% 时,氧化能力变强,以至于破坏了胶原的结构,此时的作用以降解为主。

3 结 论

1)本[illegible]提出了一套免疫原性检测方案,可以用于检测所有可植入生物材料的免疫原性,能为生物医用材料的生物安全性检测提供参考。

2)胶原膜 1 在 BALB/c 小鼠中引起了轻微的系统性免疫反应,包括脾细胞数目和活化以及 IgG 抗体分泌增多,但是与未植入材料的老鼠无具有统计学意义的差异。另外,胶原膜 1 在植入局部引起了一定的细胞浸润,即炎症。

3)胶原膜 2 在 BALB/c 小鼠中也引起了轻微的系统性免疫反应,主要是脾细胞数目增多,和 B 细胞活化增多,但是程度比胶原膜 1 要轻,还发生了反应程度比胶原膜 1 稍轻的局部炎症。

4)总体来说,2 种胶原膜在 BALB/c 小鼠中引起的免疫反应较弱,比 NC 组稍强,远远不及 PC 组,因此,这 2 种胶原膜,尤其是胶原膜 2,可被认为是安全可靠的骨修复材料,能被应用于临床试验。

致谢 感谢北京大学医学部王巍老师在实验中给予的指导与帮助,感谢谷歌生物科技有限公司给予技术支持。在此感激以上老师和单位的帮助!

参考文献（References）

[1] TSESIS I, ROSEN E, TAMSE A, et al. Effect of guided tissue regeneration on the outcome of surgical endodontic treatment: A systematic review and meta-analysis[J]. Journal of Endodontics, 2011, 37(8): 1039-1045.

[2] LEKOVIC V, CAMARGO P M, WEINLAENDER M, et al. Effectiveness of a combination of platelet-rich plasma, bovine porous bone mineral and guided tissue regeneration in the treatment of mandibular grade Ⅱ molar furcations in humans[J]. Journal of Clinical Periodontology, 2003, 30(8): 746-751.

[3] SUMITA Y, HONDA M J, OHARA T, et al. Performance of collagen sponge as a 3-D scaffold for tooth-tissue engineering[J]. Biomaterials, 2006, 27(17): 3238-3248.

[4] LU H K, LEE S Y, LIN F P. Elastic modulus, permeation time and swelling ratio of a new porcine dermal collagen membrane [J]. Journal of Periodontal Research, 1998, 33(5): 243-248.

[5] PITARU S, TAL H, SOLDINGER M, et al. Collagen membranes prevent apical migration of epithelium and support new connective tissue attachment during periodontal wound healing in dogs [J]. Journal of Periodontal Research, 1989, 24(4): 247-253.

[6] SCULEAN A, NIKOLIDAKIS D, NIKOU G, et al. Biomaterials for promoting periodontal regeneration in human intrabony defects: A systematic review[J]. Periodontol 2000, 2015, 68(1): 182-216.

[7] LYNN A K, YANNAS I V, BONFIELD W. Antigenicity and immunogenicity of collagen[J]. Journal of Biomedical Materials Research Part B: Applied Biomaterials, 2004, 71(2): 343-354.

[8] PENG Y Y, GLATTAUER V, RAMSHAW J A, et al. Evaluation of the immunogenicity and cell compatibility of avian collagen for biomedical applications[J]. Journal of Biomedical Materials Research Part A, 2010, 93(4): 1235-1244.

[9] ZIV O, AVTALION R R, MARGEL S. Immunogenicity of bioactive magnetic nanoparticles: Natural and acquired antibodies [J]. Journal of Biomedical Materials Research Part A, 2008, 85(4): 1011-1021.

[10] DILGIMEN A S, MUSTAFAEVA Z, DEMCHENKO M, et al. Water-soluble covalent conjugates of bovine serum albumin with anionic poly(n-isopropyl-acrylamide) and their immunogenicity [J]. Biomaterials, 2001, 22(17): 2383-2392.

[11] KREISER S, ECKHARDT J, KUHNT C, et al. Murine cd83-positive T cells mediate suppressor functions in vitro and in vivo [J]. Immunobiology, 2015, 220(2): 270-279.

[12] O'DONNELL H, PHAM O H, LI L X, et al. Toll-like receptor and inflammasome signals converge to amplify the innate bactericidal capacity of t helper 1 cells[J]. Immunity, 2014, 40(2): 213-224.

[13] WELCH R J, LITWIN C M. A comparison of brucella igg and igm elisa assays with agglutination methodology[J]. Journal of Clinical Laboratory Analysis, 2010, 24(3): 160-162.

[14] LIU H, WISE S G, RNJAK-KOVACINA J, et al. Biocompatibility of silk-tropoelastin protein polymers[J]. Biomaterials, 2014, 35(19): 5138-5147.

[15] LIU L, KUFFOVA L, GRIFFITH M, et al. Immunological responses in mice to full-thickness corneal grafts engineered from porcine collagen[J]. Biomaterials, 2007, 28(26): 3807-3814.

[16] PATINO M G, NEIDERS M E, ANDREANA S, et al. Cellular inflammatory response to porcine collagen membranes[J]. Journal of Periodontal Research, 2003, 38(5): 458-464.

[17] 方哲翔,王建华,袁平,等. 医用胶原修复膜病毒灭活/去除工艺的验证和评价[J]. 中国生物制品学杂志, 2016, 29(12): 1341-1345.
FANG Z X, WANG J H, YUAN P, et al. Validation and evaluation of inactivation/removal of medical collagen repair membrane[J]. Chinese Journal of Biologicals, 2016, 29(12): 1341-1345(in Chinese).

[18] 王朋. 过氧化氢消毒灭菌技术介绍[J]. 化工与医药工程, 2012, 33(6): 51-53.
WANG P. Introduction of sterilization technology with vaporized hydroge peroxide[J]. Chemical and Pharmaceutical Engineering, 2012, 33(6): 51-53(in Chinese).

[19] 龚居霞,刘新华,但卫华,等. 过氧化氢处理对Ⅰ型胶原结构和性能的影响[J]. 中国皮革, 2015(1): 10-13.
GONG J X, LIU X H, DAN W H, et al. Effects of hydrogen peroxide treatment on structure and performance of type Ⅰ collagen[J]. China Leather, 2015(1): 10-13(in Chinese).

作者简介:

张林　女,硕士研究生。主要研究方向:生物医用材料。

牛旭锋　男,博士,副教授,博士生导师。主要研究方向:生物医用材料。

Immunological response evaluation of absorbable collagen membrane in vivo

ZHANG Lin, SUN Lei, XU Menghan, NIU Xufeng*

(School of Biological Science and Medical Engineering, Beijing University of Aeronautics and Astronautics, Beijing 100083, China)

Abstract: Immune response is one of the critical factors to limit implantable biomaterials' application. In this study, two kinds of collagen membranes for bone regeneration were evaluated in terms of immunological response in vivo, which is hoped to lay foundations for clinical trials. At day 14 following subcutaneous implantation of the two membranes in BALB/c mice, compared with negative control (NC, no implant), spleen and lymph nodes showed no obvious swelling, and normal lymph nodes' cell population as well as one-fold more splenic cell population was observed. Flow cytometry analysis demonstrated that in mice with collagen membrane 1, splenic T lymphocytes percentage decreased by about 13%, but no significant change was discovered in T lymphocyte subsets; collagen membrane 2 did not trigger apparent splenic cells composition alteration; the two membranes activated one-fold more B lymphocytes than NC. Enzyme linked immunosorbent assay indicated that one-fold higher IgG concentration than NC was detected in mice with collagen membrane 1 in day 14. Lymphocytes proliferation assay in vitro did not show significant difference from NC. H&E staining of local tissues exhibited slight cell infiltration around the two membranes. The two collagen membranes have engendered mild immune response and can be applied to clinical trials.

Keywords: collagen membrane; bone regeneration; immune response; flow cytometry; inflammation

Received: 2017-04-13; **Accepted**: 2017-05-19; **Published online**: 2017-06-16 16:10

URL: kns.cnki.net/kcms/detail/11.2625.V.20170616.1610.002.html

Foundation items: National Natural Science Foundation of China (31470915); the Fundamental Research Funds for the Central Universities (YWF-17-BJ-Y-45)

* **Corresponding author**. E-mail: nxf@buaa.edu.cn